Optical excitation of carbon nanotubes

Harald O. Jeschke

Institut für Theoretische Physik
Universität Frankfurt

July 27, 2006

Carbon Nanotubes: Why are they interesting?

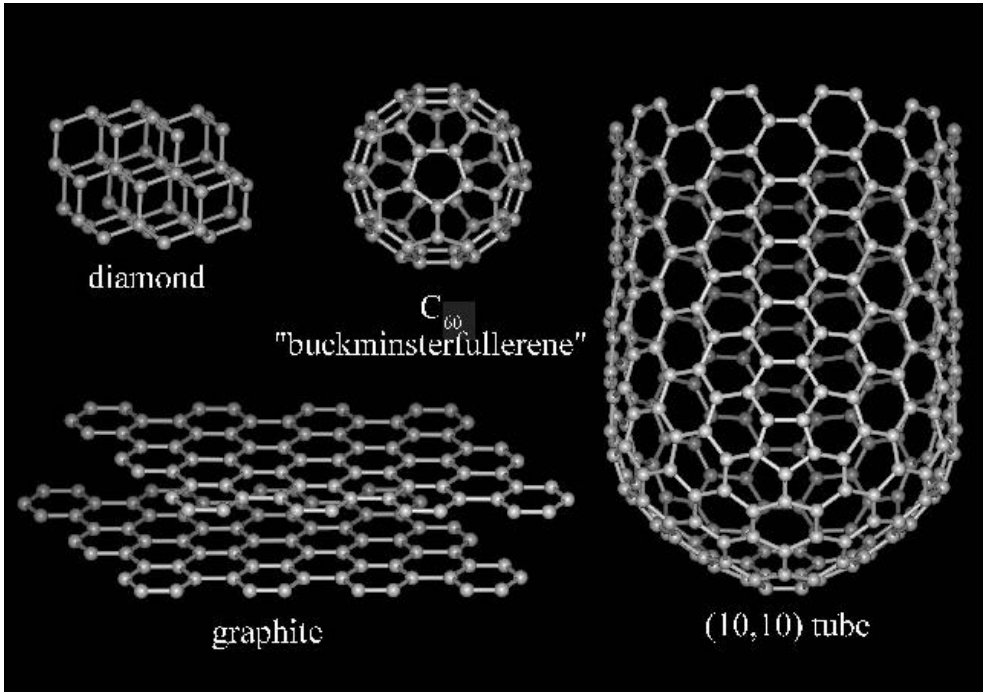

- Fully synthetic materials: Picture them as rolled up graphene sheets or as onedimensional (1D) elongated fullerenes.
- Metallic or semiconducting depending on structure.

- Realization of 1D physics.
- Unusual properties: Strongest, stiffest molecule, best molecular conductor of current and heat.
- Many open questions: Can they be produced in large quantities? Can they be grown in organized arrays or a perfect single crystal? Can they be sorted by diameter and chirality? Can they be used to make nanoelectronic devices, nanomachines?

Carbon Nanotubes: History

- Oberlin, Endo, Koyama, *Filamentous growth of carbon through benzene decomposition*, J. Cryst. Growth **32**, 335 (1976) contains early high resolution transmission electon microscope (HRTEM) images of single and multiwall carbon nanotubes, but this and similar work of the seventies and eighties was not followed up.
- The actual discovery of carbon nanotubes is credited to Iijima, Nature **354**, 56 (1991). It contains these TEM images:

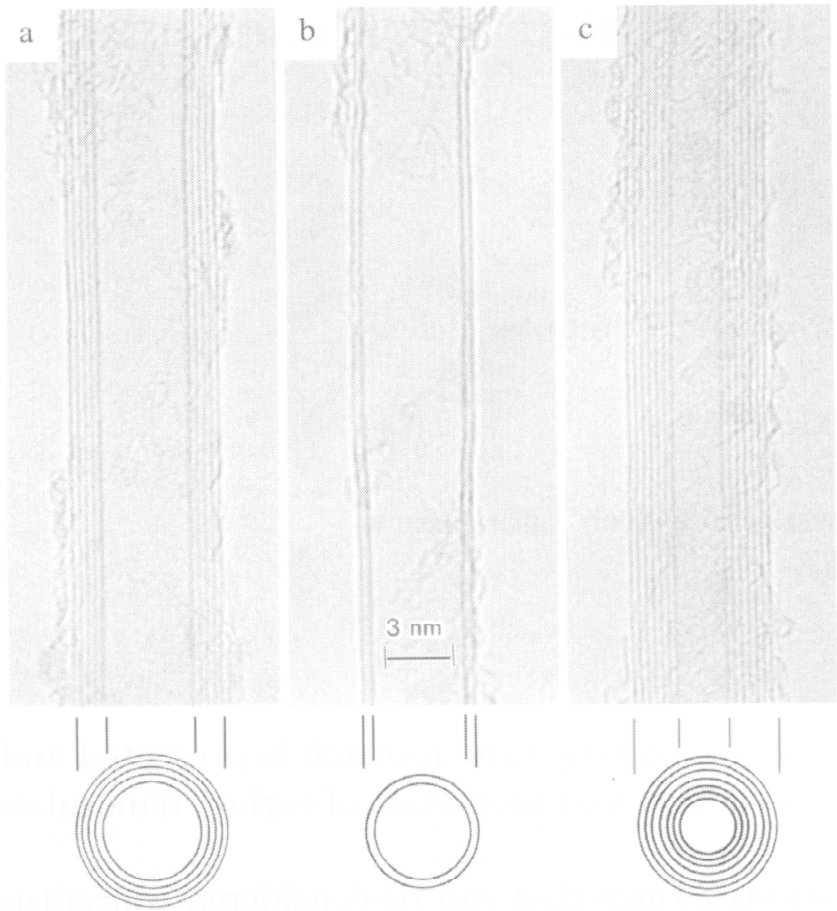

Multiwall coaxial nanotubes with various inner and outer diameters (d_i, d_o): a) $N = 5$, $d_o = 67$ Å b) $N = 2$, $d_o = 55$ Å c)$N = 7$, $d_i = 23$ Å, $d_o = 65$ Å

Electric Arc Discharge

- Arc discharge between two high purity graphite rods (6 - 10 mm diameter).
- DC current (80-100 A), He atmosphere.
- Deposit forms on cathode at a rate of 1mm/min: Cigar-like structure with dark and soft core containing carbon nanotubes (CNTs) in the form of randomly arranged multi wall nanotubes (MWNTs).
- Presence of metal catalysts (especially Ni-Y) leads to production of single wall nanotubes (SWNTs).

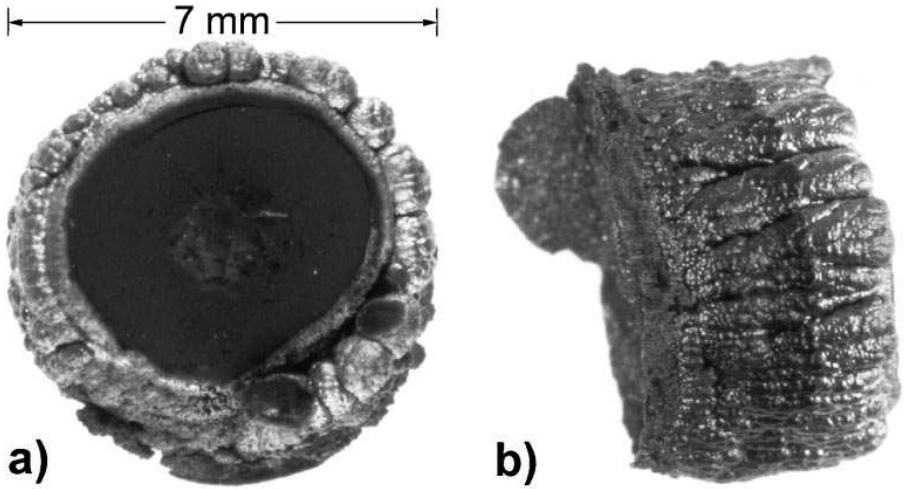

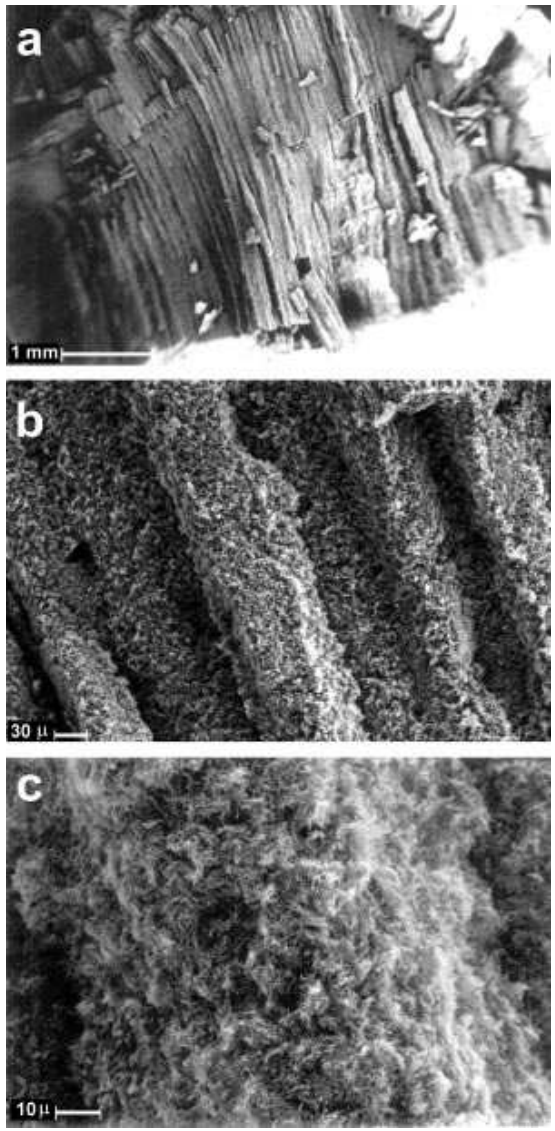

M. Terrones, Annu. Rev. Mater. Res. **33**, 419 (2003).

Laser Vaporization of Graphite Targets

- MWNTs can be generated by high-power laser vaporization of pure graphite targets in Ar atmosphere.
- Metal particles are needed as catalysts for producing SWNTs.
- Tubes are generated in bundles, typically with diameters around 14 Å.
- Scanning electron microscope (SEM) images from group of Smalley.

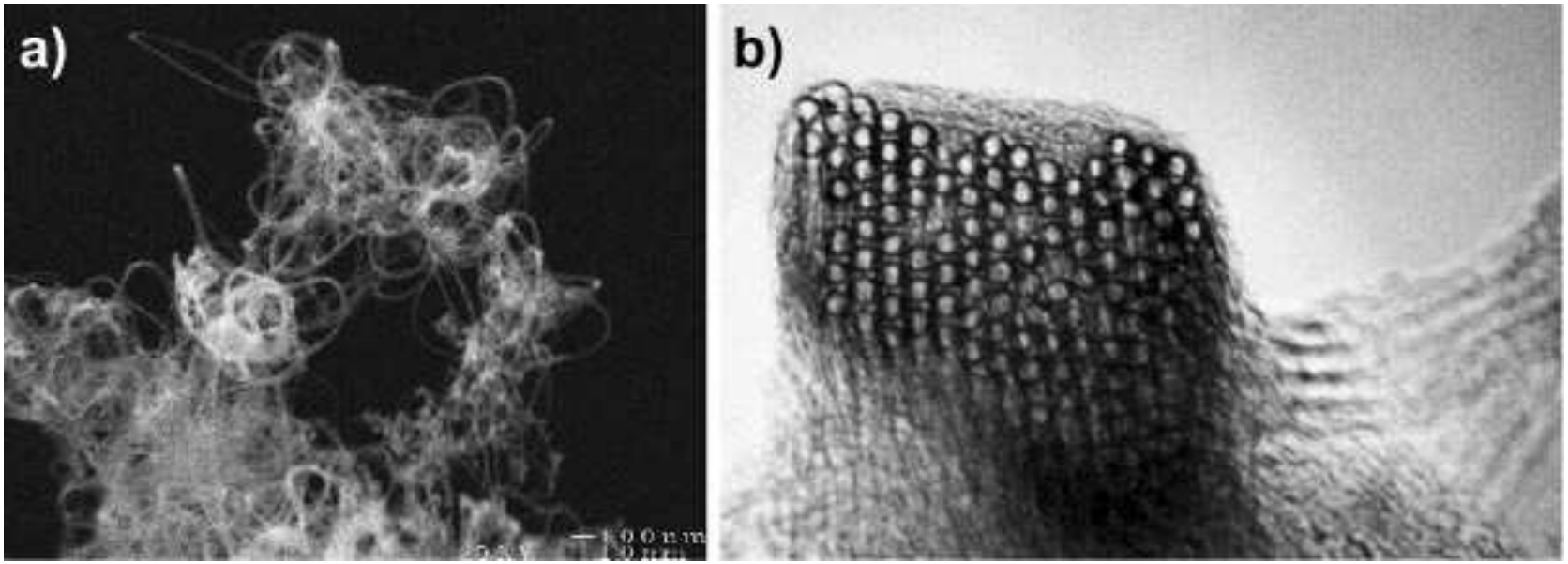

Guo, Nikolaev, Rinzler, Tomanek, Colbert and Smalley, J. Phys. Chem. **99**, 10694 (1995).

Electrolysis

- Graphite electrodes are immersed in molten LiCl (or KCl, NaCl, etc.) at temperatures above 600 °C.
- Possible growth mechanism: Carbon is dissolved in the form of Li_2C_2:

$$2Li^+ + 2e^- + 2C_{graphite} \rightarrow Li_2C_2$$

- Li_2C_2 then decays at the electrodes to form nanotubes.
- Transmission electron microscope (TEM) images from Sussex group.

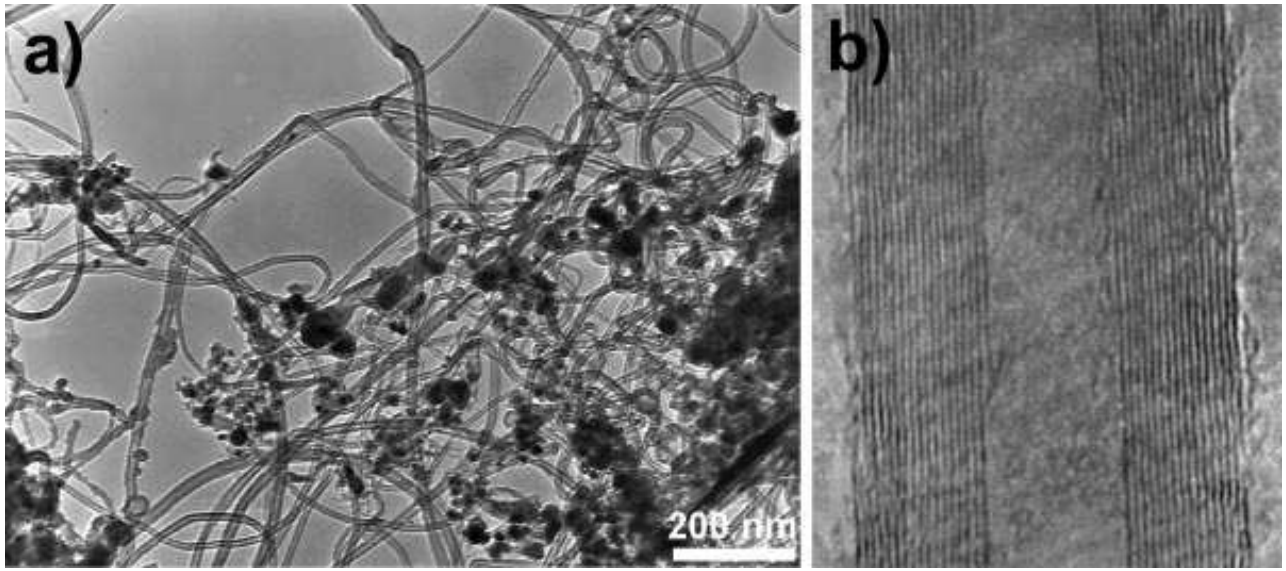

Hsu, Terrones, Terrones, Grobert, Zhu *et al.*, Chem. Phys. Lett. **301**, 159 (1999).

Chemical vapor deposition (CVD)

- Hydrocarbons are decomposed by pyrolysis over metal catalysts (Co, Ni, Fe, Pt deposited on substrates like silicon, graphite, silica).

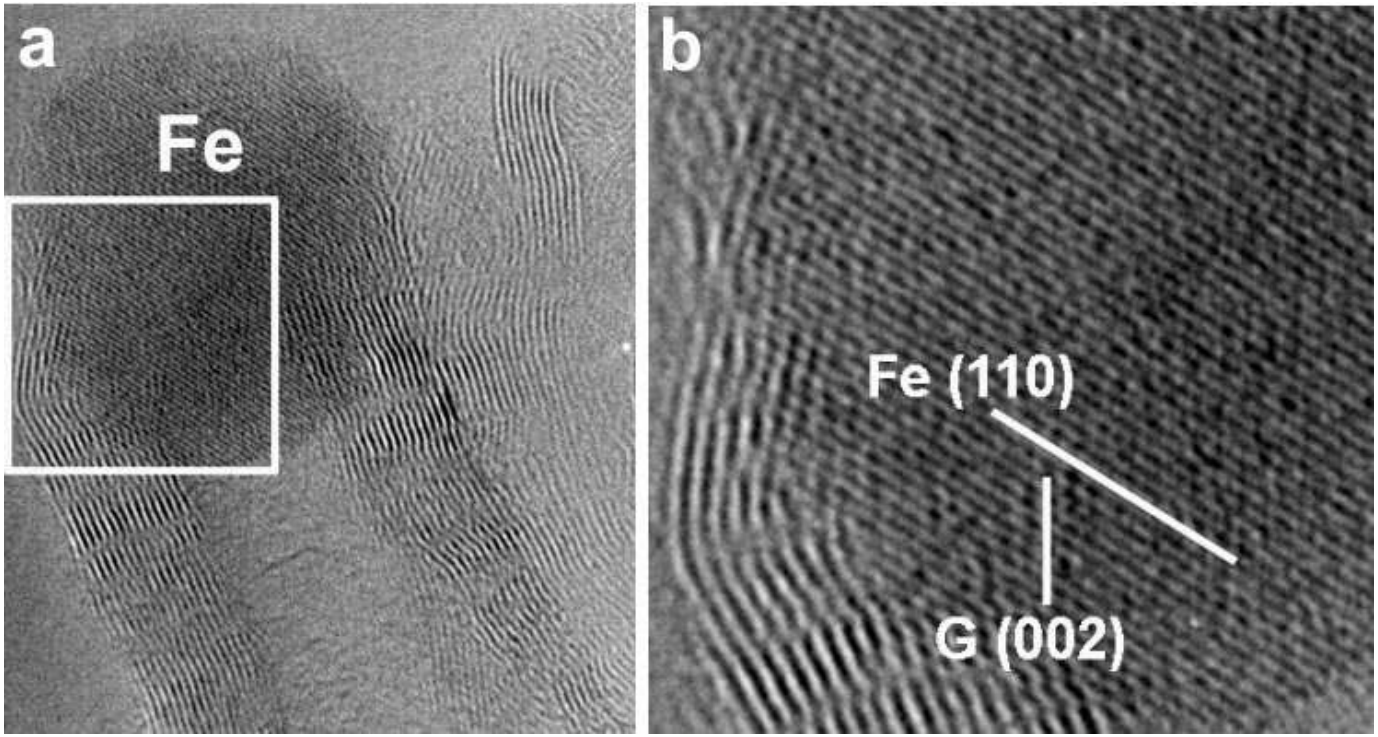

- CVD processes are used for the production of large quantities of CNTs.
- A process called HipCo involves thermolysis of $Fe(CO)_5$ in presence of carbon monoxide at elevated pressures (10 atm) and is reported to be very efficient.

M. Terrones, Annu. Rev. Mater. Res. **33**, 419 (2003).

Purification

- As result of most CNT production processes, samples contain amorphous carbon particles, spherical fullerenes, catalyst particles and other impurities. ⇒ Purification and isolation of the targeted SWNT or MWNT species important.
- Some methods rely on heating of the sample in presence of oxygen, leading to oxidation of less stable carbon structures. A problem is high weight loss (see image).
- Other methods rely on creating colloidal suspensions and filtration. This can be assisted by ultrasound.
- Boiling samples in acid can (partly) remove metal catalysts.
- Oxidation at 350 °C with gold clusters as catalysts can remove unwanted carbon structures.

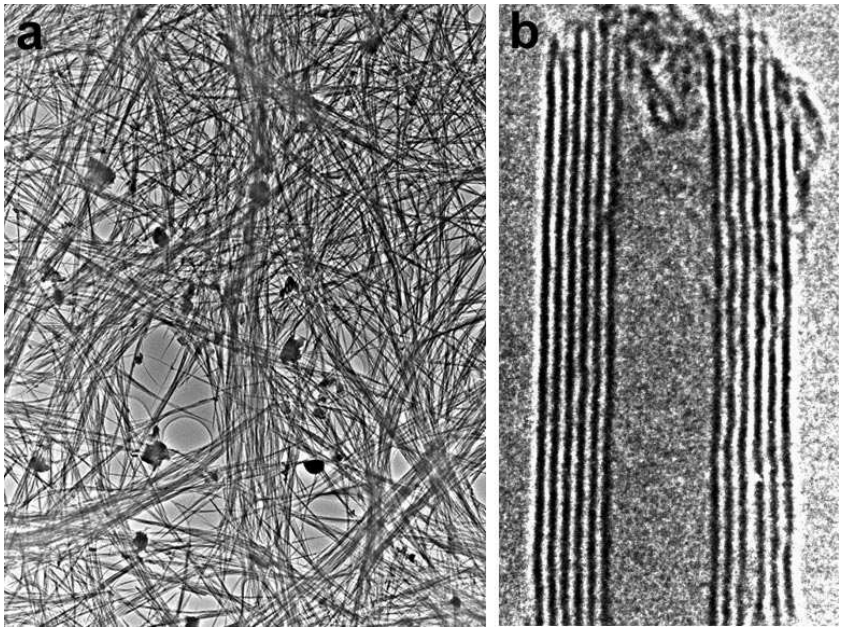

Ebbesen, Ajayan, Hiura, Tanigaki, Nature **367**, 519 (1994).

Alignment

- For many applications, aligned bundles of CNTs are needed.
- Alignment can be achieved mechanically (directional rubbing of CNTs on substrates), but more efficient are controlled growth conditions.
- Printed catalyst patterns on a substrate in combination with CVD can yield perfectly aligned MWNT arrays.

Image: Fe catalysts on crystalline Si, ethylene pyrolysis.

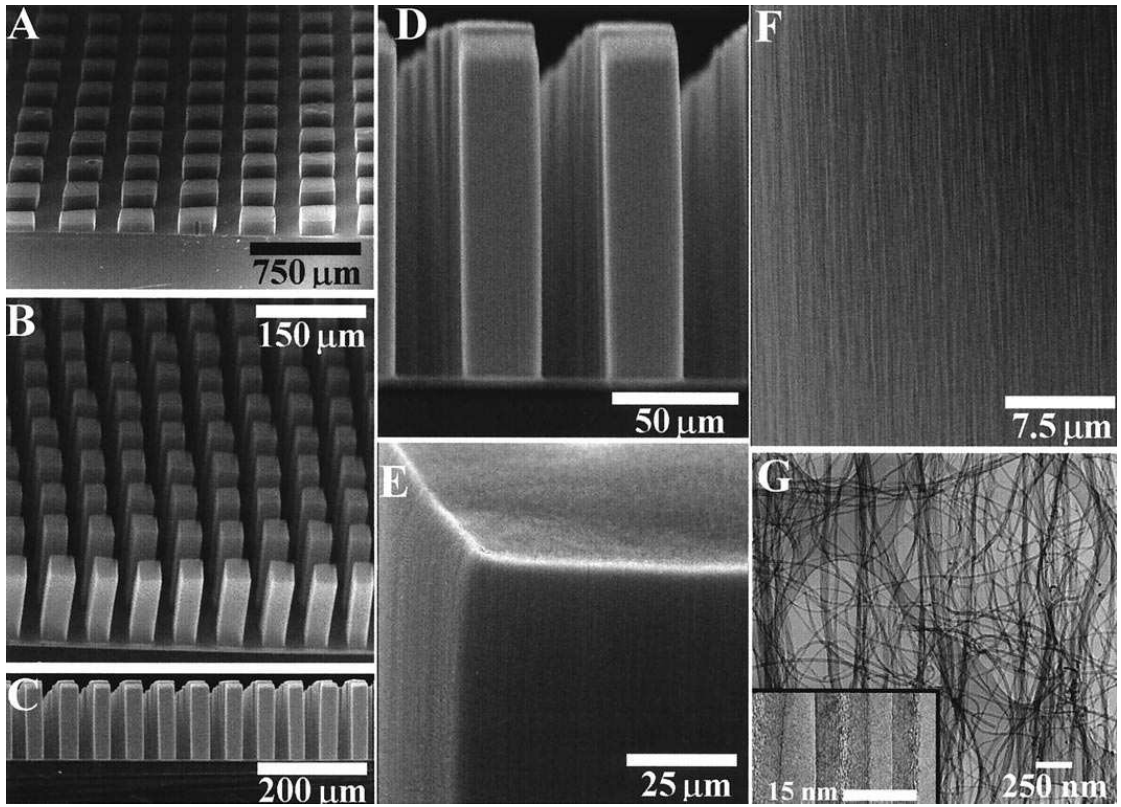

Fan, Chapline, Franklin, Tombler, Cassell, Dai, Science **283**, 512 (1999).

Structure of carbon nanotubes

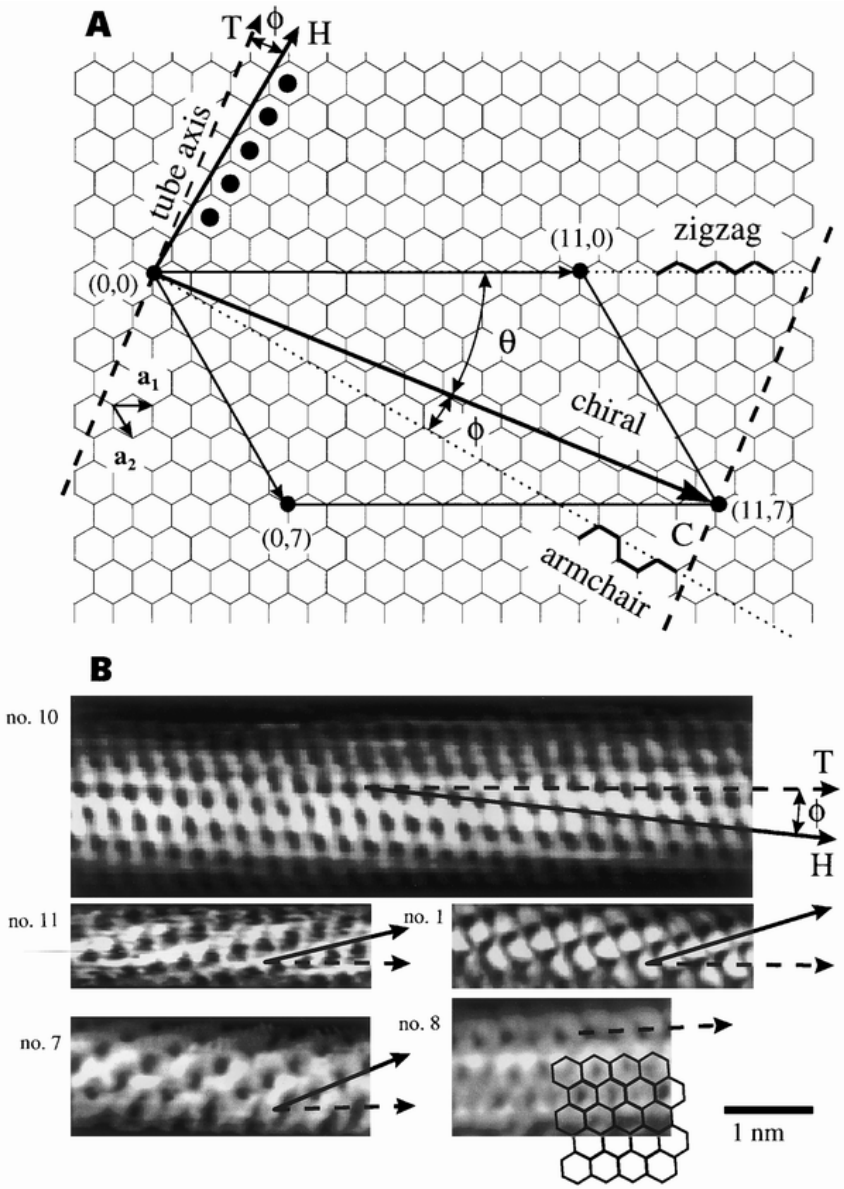

- Graphene sheet is rolled up along wrapping vector **C** so that equivalent points (0,0) and (11,7) coincide.
- **T** is perpendicular to **C** and points along the tube axis.
- **H** is perpendicular to the armchair direction and gives the direction of nearest-neighbour hexagon rows.
- θ is the angle relative to the zigzag direction.

Wilder, Venema, Rinzler, Smalley, Dekker, Nature **391**, 59 (1998).

Geometry of carbon nanotubes

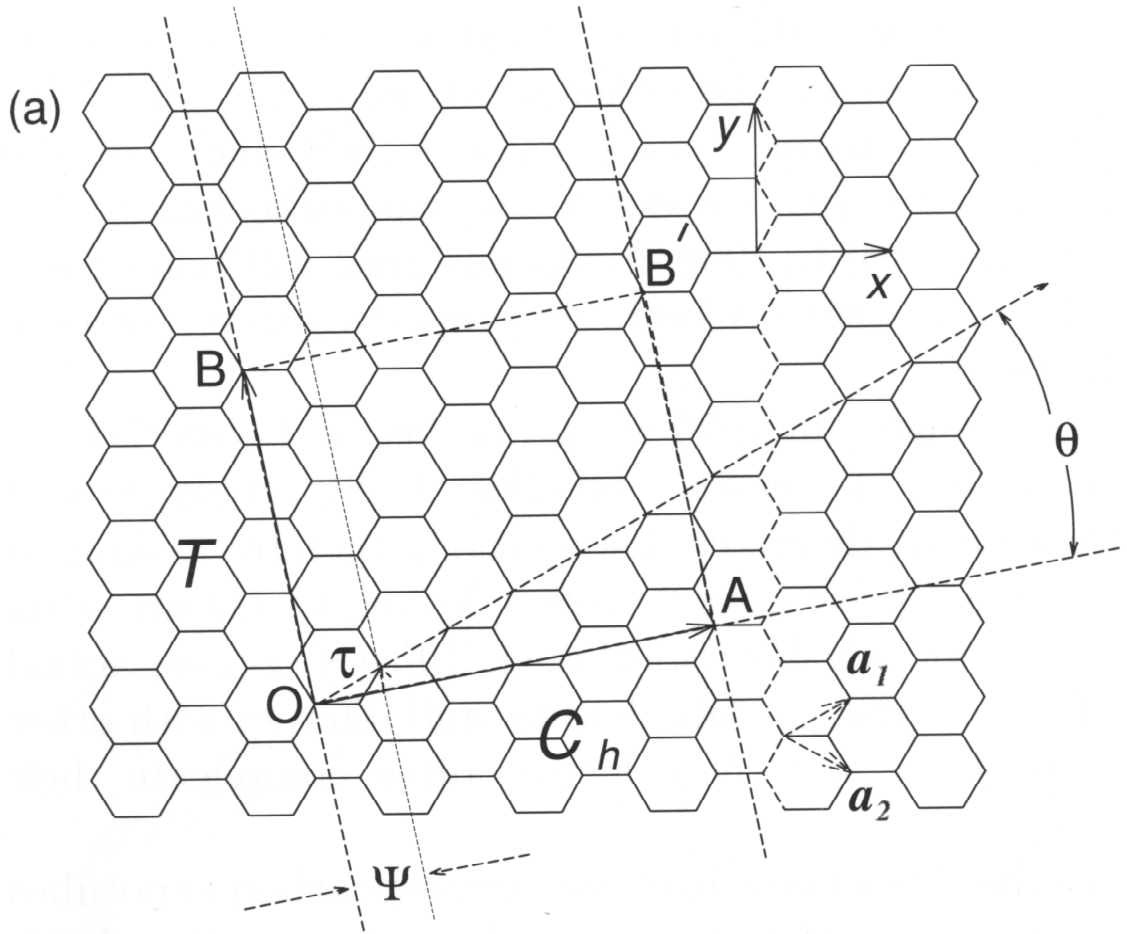

- Chiral vector $\mathbf{C}_h$ is denoted by (n, m), the socalled Hamada indices (after Hamada, Sawada, Oshiyama, Phys. Rev. Lett. **68**, 1579 (1992)).
- In terms of the unit vectors $\mathbf{a}_1$ and $\mathbf{a}_2$ of the hexagonal honeycomb lattice of the graphene sheet, it is

$$\mathbf{C}_h = n\mathbf{a}_1 + m\mathbf{a}_2$$

M.S. Dresselhaus, G. Dresselhaus, Ph. Avouris (Eds.), *Carbon Nanotubes: Synthesis, Structure, Properties and Applications*, Springer 2001.

Geometry of carbon nanotubes

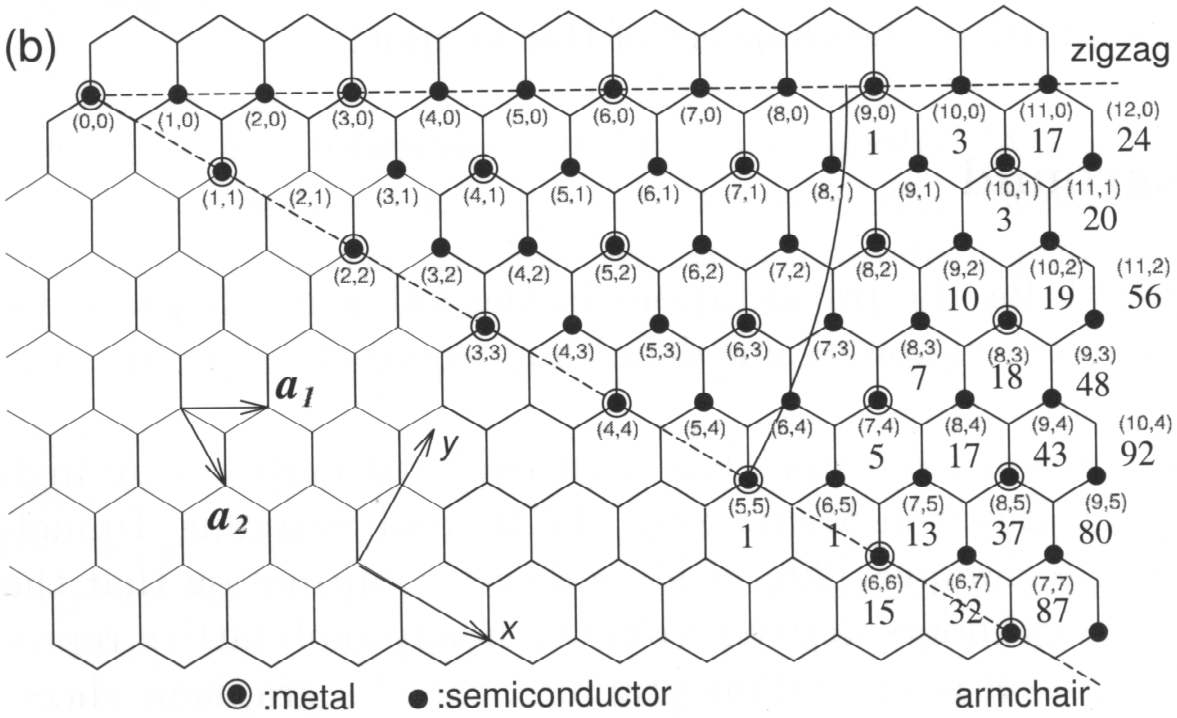

- Vectors $(n, 0)$ or $(0, m)$ denote zigzag nanotubes, vectors (n, n) denote armchair nanotubes. All other vectors (n, m) correspond to chiral nanotubes.

- The nanotube diameter d_t is given by

$$d_t = \frac{\sqrt{3} a_{C\text{-}C}}{\pi} \sqrt{m^2 + mn + n^2}$$

with carbon-carbon bond length $a_{C\text{-}C} = 1.42$ Å.

- The chiral angle θ is given by

$$\theta = \tan^{-1} \frac{\sqrt{3} n}{2m + n}$$

Thus, for the (n, n) tube, $\theta = \tan^{-1}[1/\sqrt{3}] = 30°$.

One-dimensional electronic structure

Tight binding Hamiltonian

$$\mathcal{H} = \sum_{\mathbf{i}} \varepsilon_{\mathbf{i}} |\mathbf{i}\rangle\langle\mathbf{i}| + \sum_{\mathbf{ij}} V_{ij} |\mathbf{i}\rangle\langle\mathbf{j}|$$

where $|\mathbf{i}\rangle$ is an atomic-like orbital centered at site $\mathbf{i}$. $\varepsilon_{\mathbf{i}}$ are the on-site energies, V_{ij} are called hopping integrals.

By substitution into the Schrödinger equation $\mathcal{H}|\psi\rangle = E|\psi\rangle$, one can confirm that the eigenfunctions and eigenvalues of the Hamiltonian are

$$|\mathbf{k}\rangle = \frac{1}{\sqrt{N}} \sum_{\mathbf{i}} e^{i\mathbf{k}\mathbf{i}} |\mathbf{i}\rangle$$

and

$$E(\mathbf{k}) = \varepsilon_0 + \sum_{\mathbf{l}} V_{0\mathbf{l}} e^{i\mathbf{k}\mathbf{l}}$$

where the simple case of equal on-site energies $\varepsilon_{\mathbf{i}} = \varepsilon_0 \forall \mathbf{i}$ is assumed. In the simple case of only nearest neighbour hopping ($V_{ij} = V$ for neighboring sites, $V_{ij} = 0$ otherwise), the energy reads

$$E(\mathbf{k}) = \varepsilon_0 + V \tilde{\sum_{\mathbf{l}}} e^{i\mathbf{k}\mathbf{l}}$$

where the tilde indicates summation only over neighbours of the origin.

One-dimensional dispersion

In the one-dimensional case, this becomes (with lattice constant a)

$$E(k) = \varepsilon_0 + 2V\cos(ka)$$

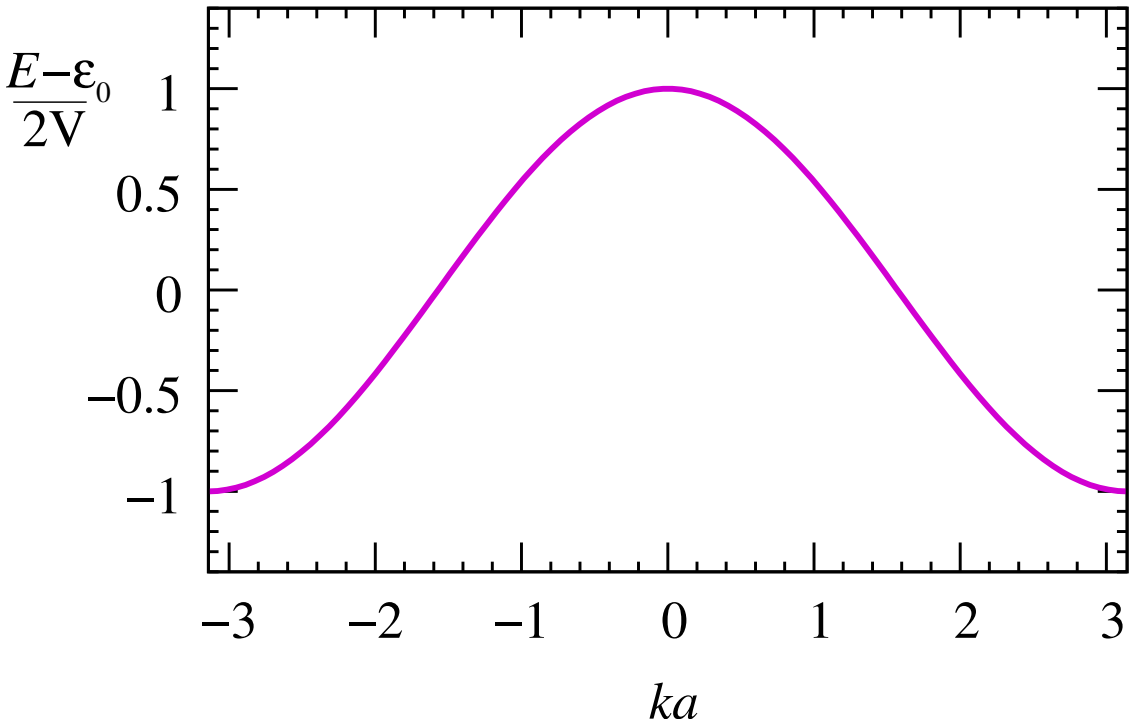

Energy E versus k with k restricted to the first Brillouin zone $-\pi/a \leq k \leq \pi/a$.

Thus, the allowed states form a band extending from $E = \varepsilon_0 - 2V$ to $E = \varepsilon_0 + 2V$ with half band width $2V$. Similarly, the energy in the two-dimensional case (2D square lattice) reads

$$E(\mathbf{k}) = \varepsilon_0 + 2V\big[\cos(k_1 a) + \cos(k_2 a)\big]$$

and in the three-dimensional case (3D simple cubic lattice)

$$E(\mathbf{k}) = \varepsilon_0 + 2V\big[\cos(k_1 a) + \cos(k_2 a) + \cos(k_3 a)\big]$$

One-dimensional non-interacting Greens function

The Greens function for the tight binding Hamiltonian reads

$$G(z) = \sum_{\mathbf{k}} \frac{|\mathbf{k}\rangle\langle\mathbf{k}|}{z - E(\mathbf{k})}$$

Its matrix elements are

$$G(\mathbf{l}, \mathbf{m}; z) = \langle \mathbf{l}|G(z)|\mathbf{m}\rangle = \sum_{\mathbf{k}} \frac{\langle \mathbf{l}|\mathbf{k}\rangle\langle\mathbf{k}|\mathbf{m}\rangle}{z - E(\mathbf{k})} = \frac{\Omega}{N(2\pi)^d} \int_{\text{1st Brillouin zone}} d\mathbf{k} \frac{e^{i\mathbf{k}(\mathbf{l}-\mathbf{m})}}{z - E(\mathbf{k})}$$

In particular, in one dimension this reads

$$G(l, m; z) = \frac{L}{N2\pi} \int_{-\pi/a}^{\pi/a} dk \frac{e^{ika(l-m)}}{z - \varepsilon_0 - 2V\cos(ka)} = \frac{1}{2\pi} \int_{-\pi}^{\pi} d\phi \frac{e^{i\phi(l-m)}}{z - \varepsilon_0 - 2V\cos\phi}$$

Performing the integration via a contour integration and with the method of residues yields

$$G^{\pm}(l, m; E) = \frac{\mp i}{\sqrt{(2V)^2 - (E - \varepsilon_0)^2}} (x \mp i\sqrt{1 - x^2})^{|l-m|}$$

where $\varepsilon_0 - 2V < E < \varepsilon_0 + 2V$ and $x = (E - \varepsilon_0)/2V$.

One-dimensional density of states

Then the density of states (DOS) per site is

$$\rho(E) = \mp\frac{1}{\pi}\mathrm{Im}\{G^{\pm}(I,I;E)\} = \frac{\theta(2V - |E-\varepsilon_0|)}{\pi\sqrt{(2V)^2 - (E-\varepsilon_0)^2}}$$

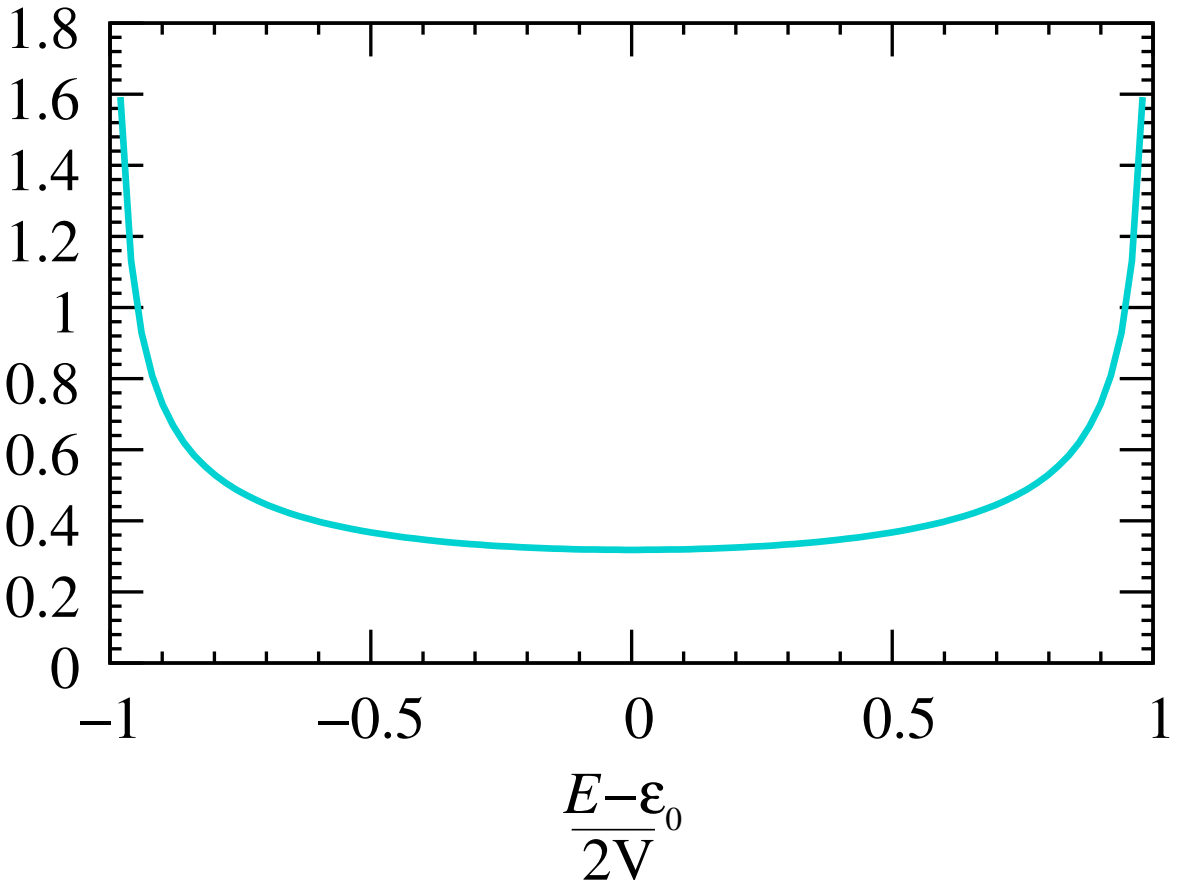

The DOS shows van Hove singularities at the band edges which are typical of one-dimensional systems.

For more details see E.N. Economou, Green's Functions in Quantum Physics, Springer 1990.

Carbon densities of states

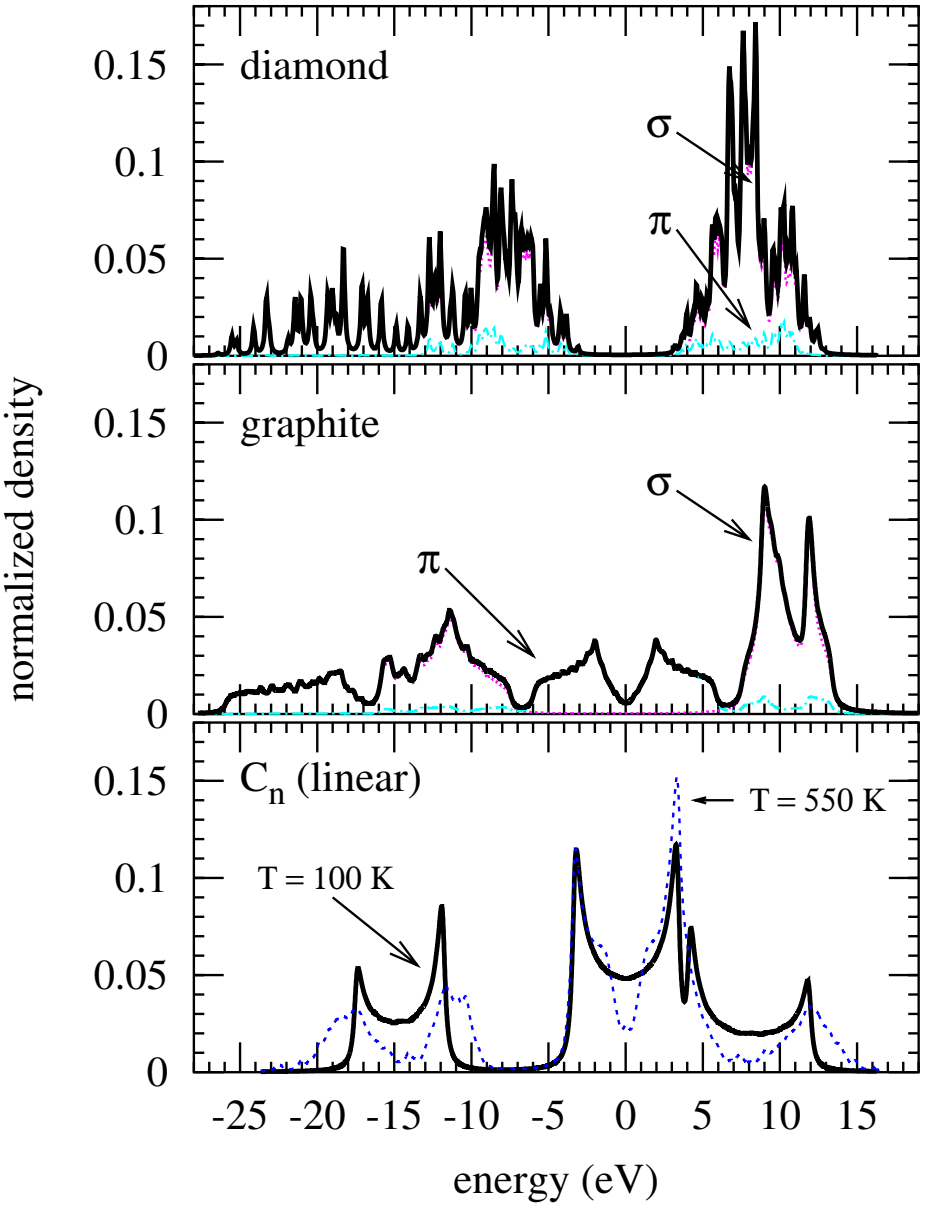

DOS of diamond, graphite and linear carbon chains calculated with an sp^3 tight binding scheme.

For details see H. O. Jeschke and M. E. Garcia, *Ultrafast structural changes induced by femtosecond laser pulses*, in B.W. Adams (ed.), *Nonlinear Optics, Quantum Optics and Ultrafast Phenomena with X-rays*, Kluwer Academic Publishers, Boston/Dordrecht/London, June 2003.

Carbon nanotubes: DOS from conductivity measurements

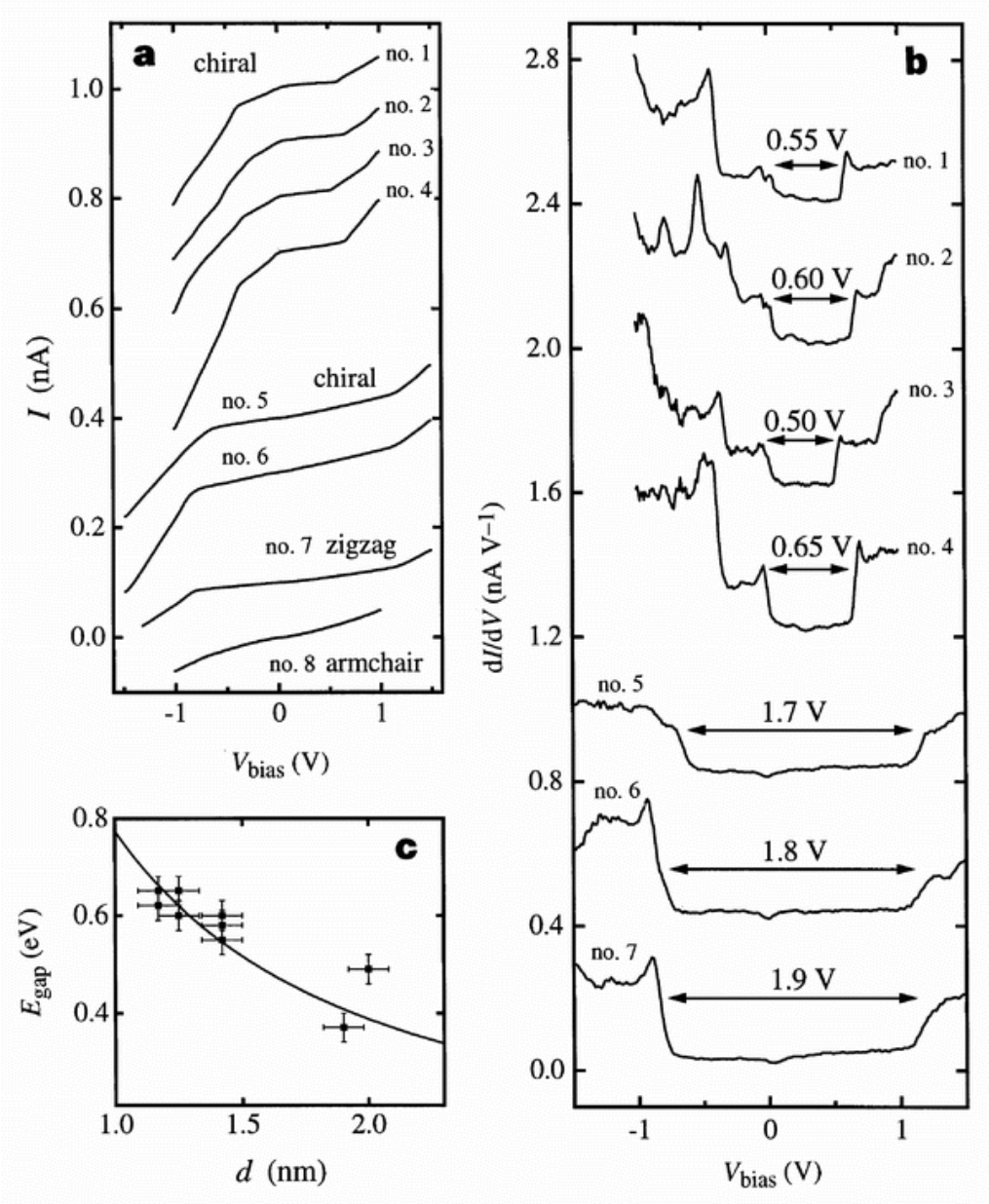

- Scanning tunneling spectroscopy (STS) measurements of current as a function of applied voltage.
- Differential conductance dI/dV can be considered proportional to the DOS.
- Small gaps (1-4) interpreted as semiconducting, large gaps (5-7) as metallic.

Wilder, Venema, Rinzler, Smalley, Dekker, Nature **391**, 59 (1998).

Carbon nanotubes: DOS from conductivity measurements

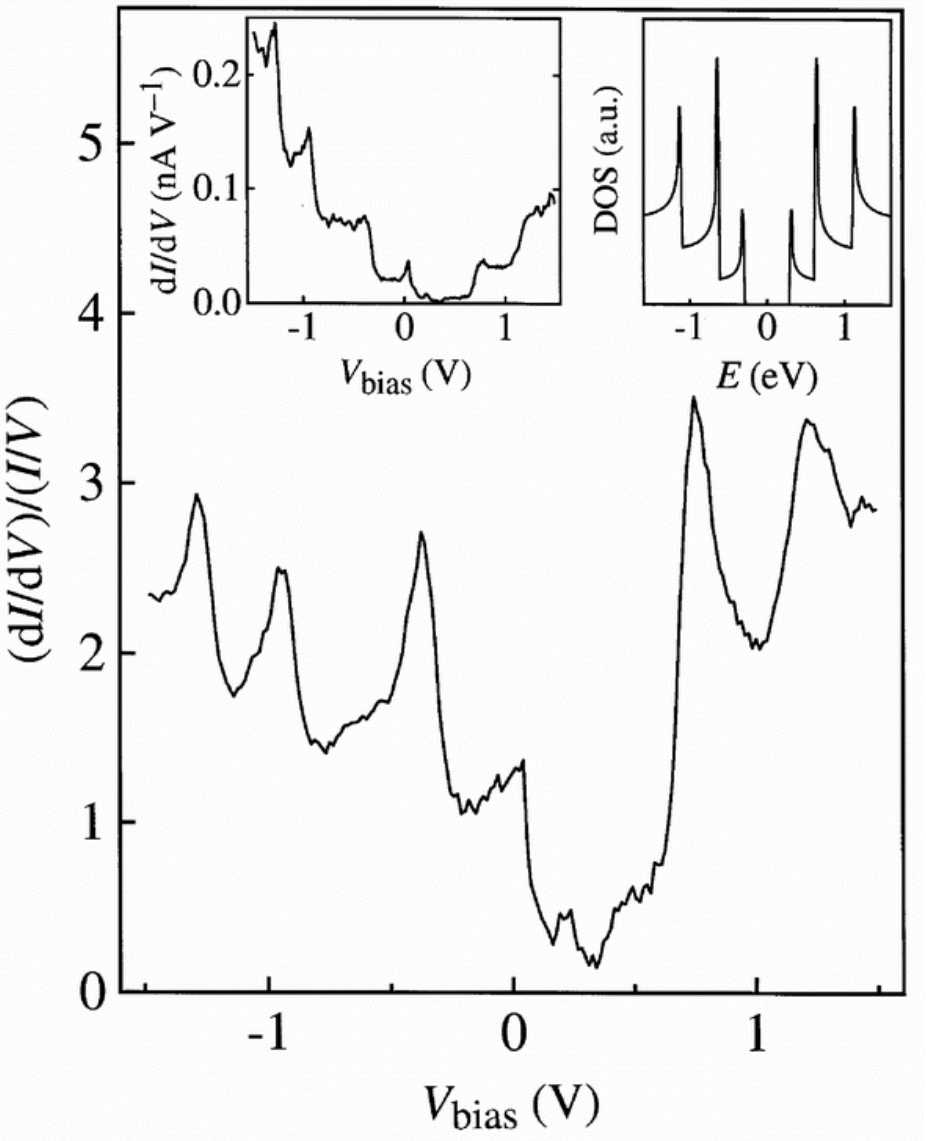

- Differential conductance normalized by total conductivity $(dI/dV)/(I/V)$ is considered a better measure of the DOS as it removes some artifacts of the scanning tunneling microscope (see Stroscio, Feenstra, Fein, Phys. Rev. Lett. **57**, 2579 (1986)).
- Sharp van Hove singularities as in the calculated DOS for a (16,0) tube, but broadening and asymmetry are attributed to a substrate influence.

Carbon nanotubes: DOS from conductivity measurements

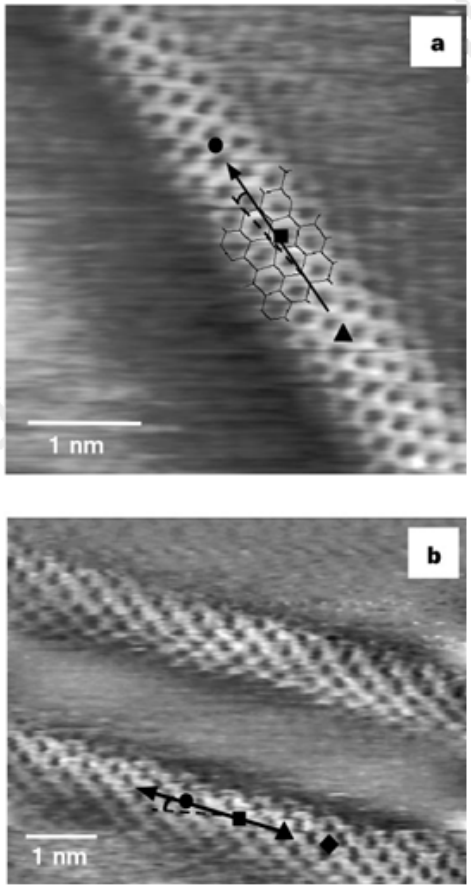

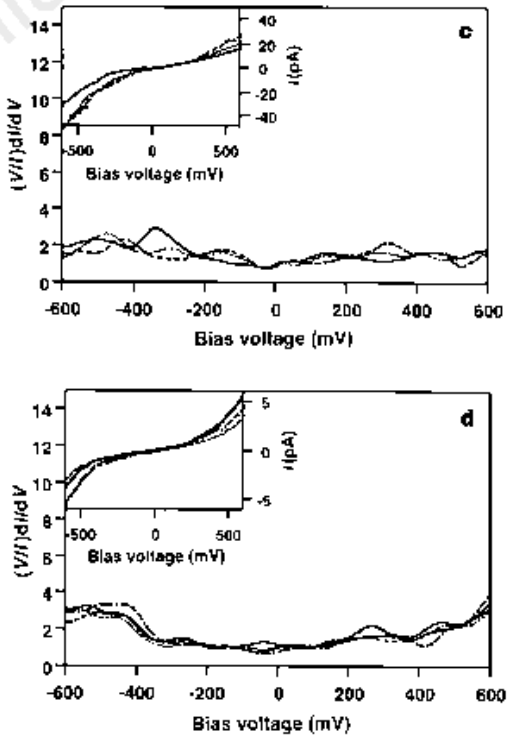

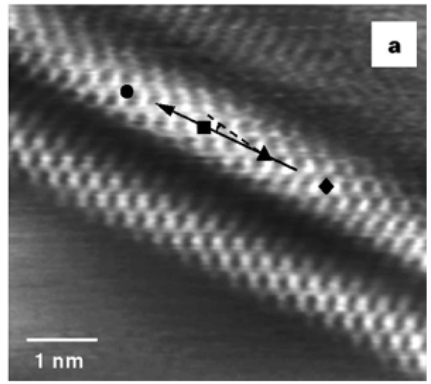

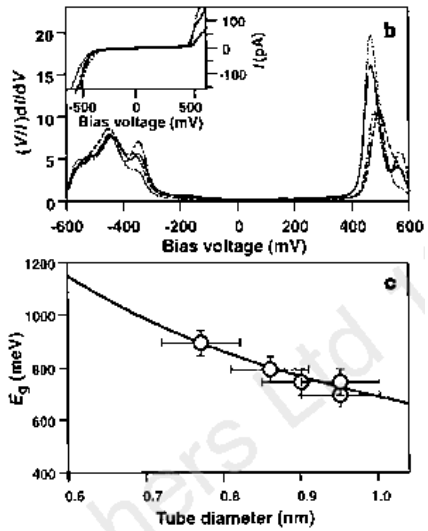

Metallic (left) and semiconducting DOS from normalized differential conductance measurements by a different group. Gap fitted with $E_{\text{gap}} = 2\gamma_0 a_{\text{C-C}}/d$.

Odom, Huang, Kim, Lieber, Nature **391**, 62 (1998).

Predicted electronic structure of carbon nanotubes

- Description with the minimal model of only valence π and conduction π^* energy bands of graphite and nanotubes.
- (2×2) Hamiltonian $\mathcal{H}$ and overlap integral matrix $\mathcal{S}$, for the two inequivalent atoms in 2D graphite:

$$\mathcal{H} = \begin{pmatrix} \varepsilon_{2p} & -\gamma_0 f(k) \\ -\gamma_0 f(k)^* & \varepsilon_{2p} \end{pmatrix} \qquad \mathcal{S} = \begin{pmatrix} 1 & sf(k) \\ sf(k)^* & 1 \end{pmatrix}$$

with on-site energy ε_{2p} and

$$f(k) = e^{ik_x a/\sqrt{3}} + 2e^{-ik_x a/2\sqrt{3}} \cos\frac{k_y a}{2} \quad \text{with} a = |\mathbf{a}_1| = |\mathbf{a}_2| = \sqrt{a_{\text{C-C}}}$$

- Solution of the secular equation $\det(\mathcal{H} - E\mathcal{S}) = 0$ leads to the eigenvalues

$$E^{\pm}_{g2\text{D}}(\mathbf{k}) = \frac{\varepsilon_{2p} \pm \gamma_0 w(\mathbf{k})}{1 \mp s w(\mathbf{k})}$$

for the C-C hopping energy γ_0 and the overlap s of wave functions on adjacent sites. $w(\mathbf{k})$ is given by

$$w(\mathbf{k}) = \sqrt{|f(\mathbf{k})|^2} = \sqrt{1 + 4\cos\frac{\sqrt{3}k_x a}{2}\cos\frac{k_y a}{2} + 4\cos^2\frac{k_y a}{2}}$$

Saito, Dresselhaus, Dresselhaus, Phys. Rev. B **61**, 2981 (2000).

Predicted electronic structure of carbon nanotubes

→ Near the K point, $w(\mathbf{k})$ can be approximated as linear function in $k = |\mathbf{k}|$

$$w(\mathbf{k}) \approx \frac{\sqrt{3}}{2} ka \qquad \text{for} \quad ka \ll 1$$

and thus $E(k) = \pm 3/2 \gamma_0 k a_{\text{C-C}}$.

→ Contour plot of 2D electronic energy of graphite with $s = 0$ and $\epsilon_{2p} = 0$. High symmetry points $K = (0, 4\pi/3a)$, $M = (2\pi\sqrt{3}a, 0)$ and $\Gamma = (0, 0)$.

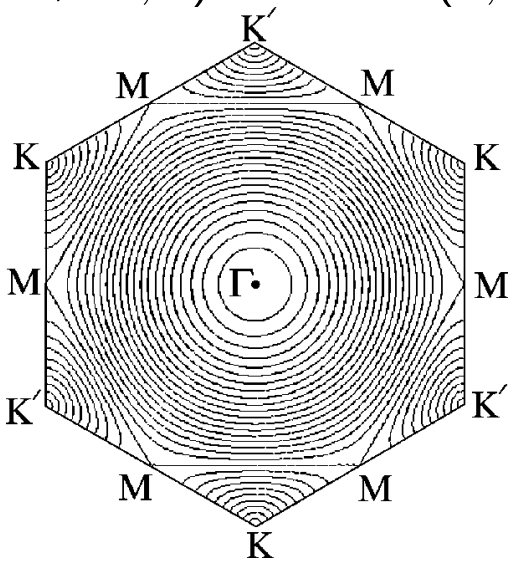

→ 2D energy dispersion relations for graphite with $\gamma_0 = 3.013$, $s = 0.129$ and $\varepsilon_{2p} = 0$. Inset shows energy dispersion along the high symmetry lines.

→ Valence π bands and conduction π^* bands are degenerate at the K points in the hexagonal Brillouin zone which corresponds to the Fermi level.

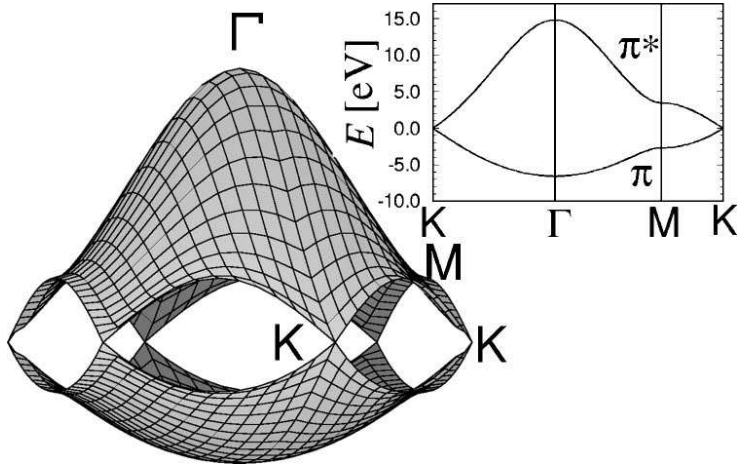

Predicted electronic structure of carbon nanotubes

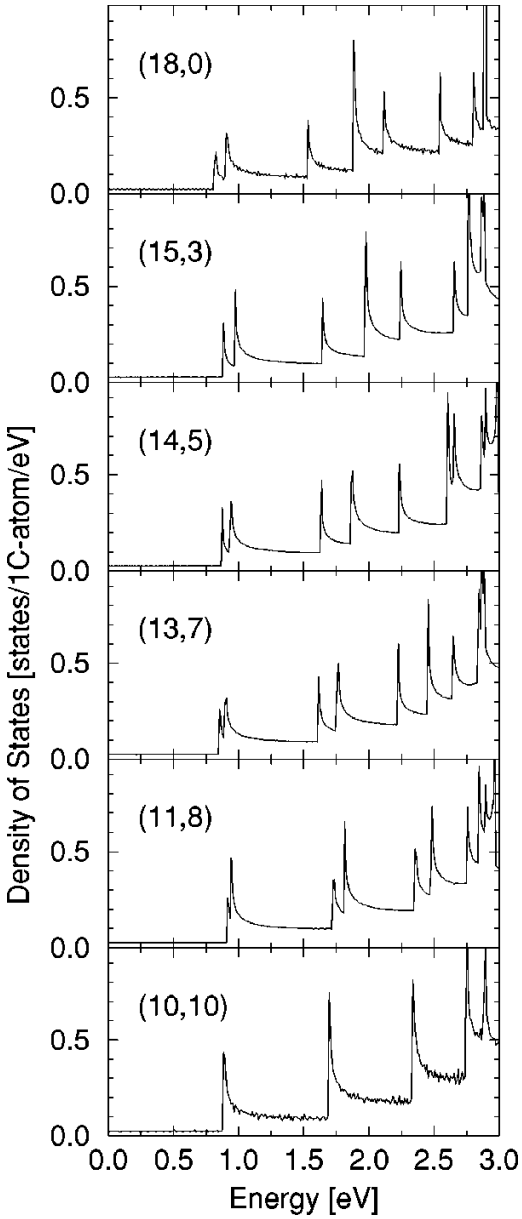

Left: 1D electronic DOS for several metallic nanotubes of approximately the same diameter, showing the effect of the chirality on the van Hove singularities.

Right: Finite diameter leads to discrete k values in K_1 direction. CNT is metallic if wave vector k (bold lines) hits K point at Fermi energy of graphite. For semiconducting nanotubes, K point is at 1/3 of the distance between bold lines.

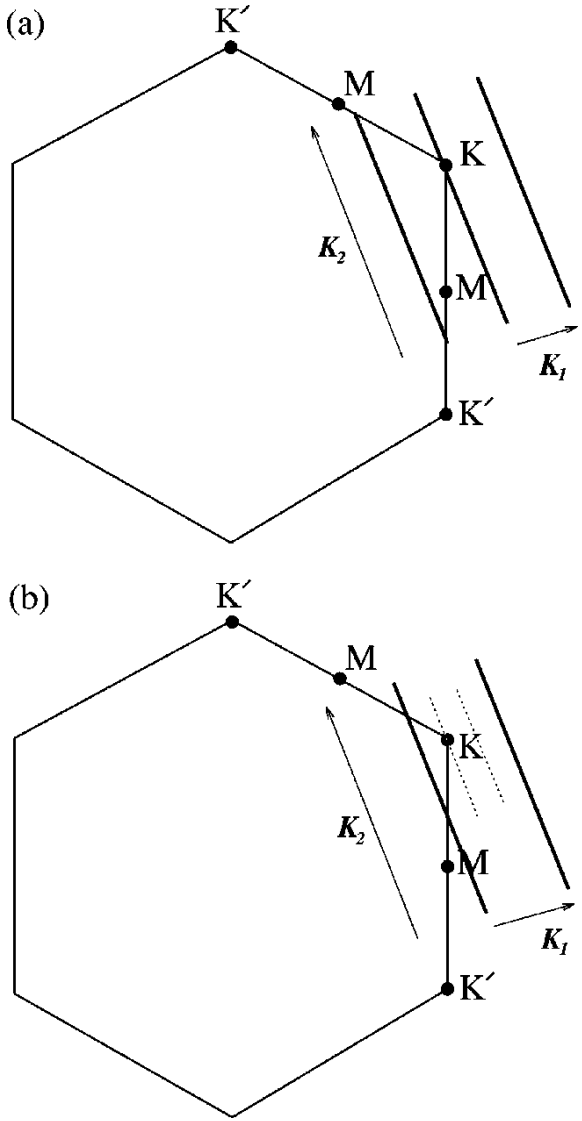

Predicted electronic structure of carbon nanotubes

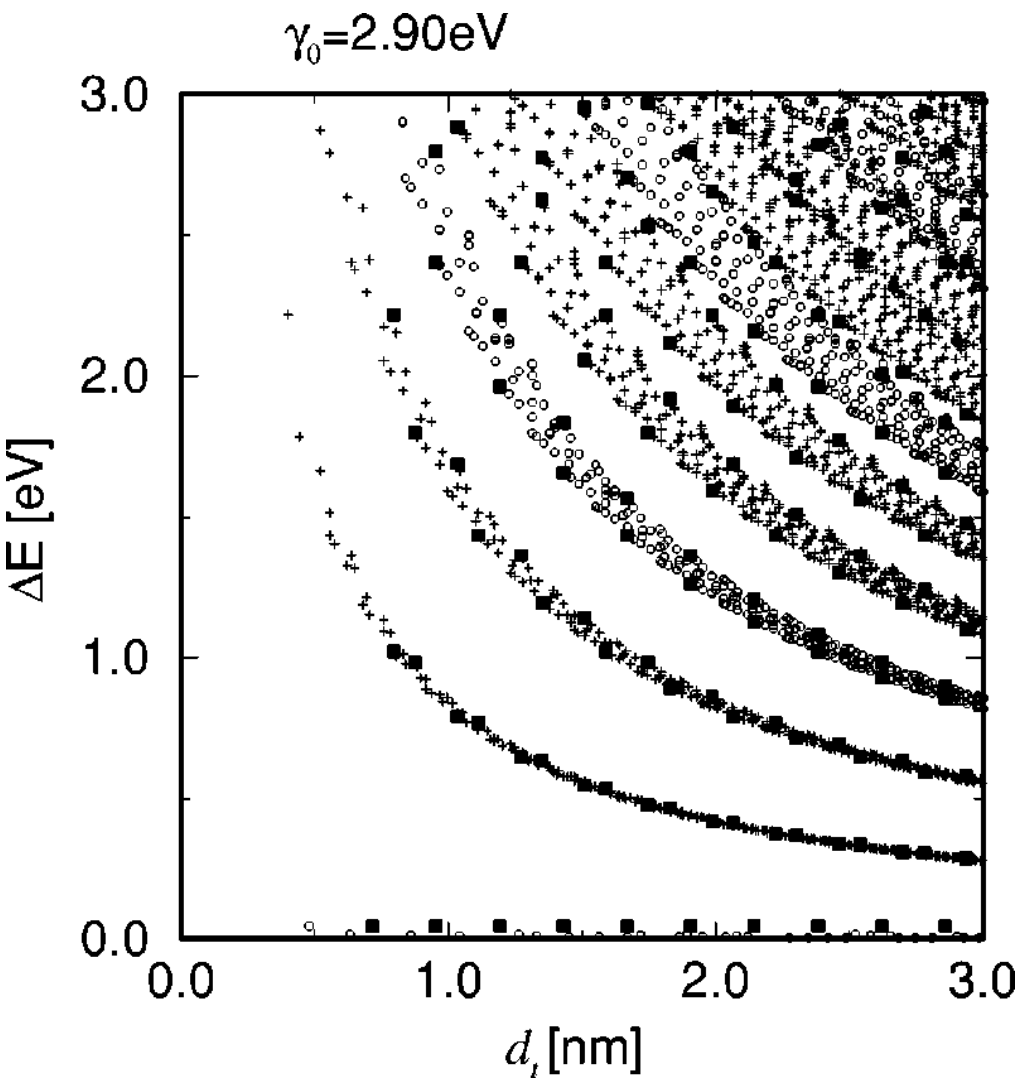

- Calculated energy separations $E_{pp}(d_t)$ between highest-lying valence-band singularity and lowest-lying conduction band singularity in the 1D DOS for all (n, m) values as a function of nanotube diameter between $0.7 < d_t < 3.0$ nm.
- Order $p = 1, 2, ..$ of valence and conduction bands symmetrically located wrt Fermi energy. $\circ \equiv$ metallic, $+ \equiv$ semiconducting, $\blacksquare \equiv$ zigzag CNT.

Carbon nanotubes: DOS observations

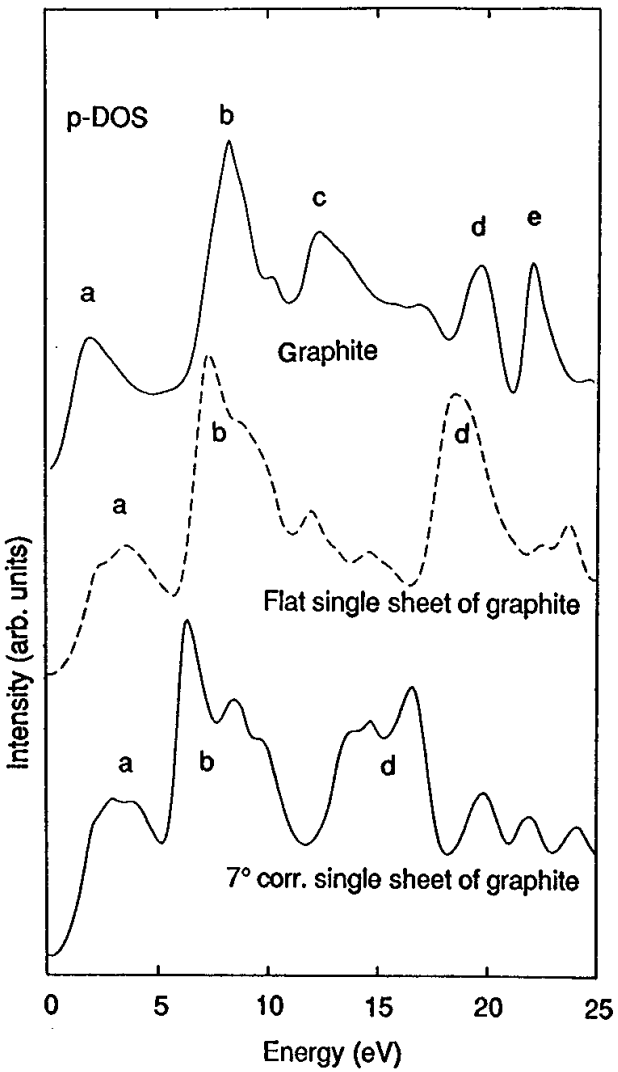

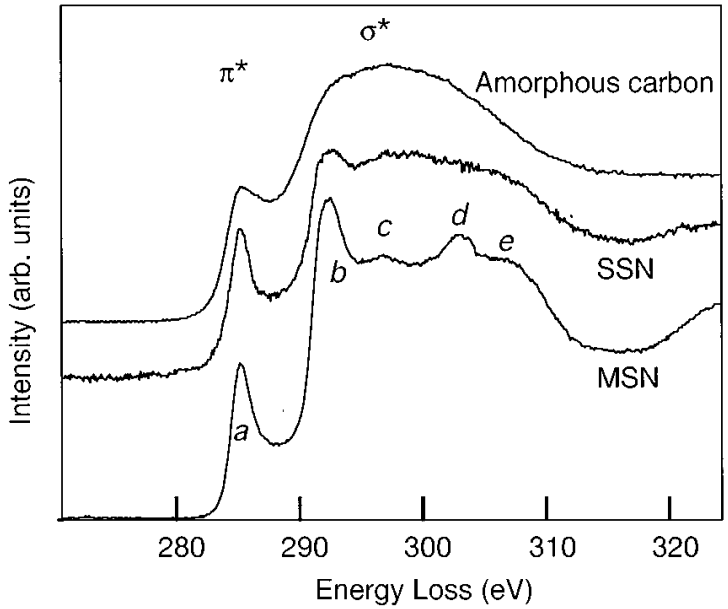

Left: *p* electron density of states calculated with *ab-initio* linear muffin-tin orbital (LMTO) method.

Right: Energy loss near-edge structures (ELNES) from electron energy loss spectroscopy (EELS).

Spectra are obtained from core electrons (in this case carbon 1*s* electrons (K edge)) excited to free states above the Fermi level.

Stéphan, Ajayan, Colliex, Cyrot-Lackmann, Sandré, Phys. Rev. B **53**, 13824 (1996).

Calculated band structure of carbon nanotubes

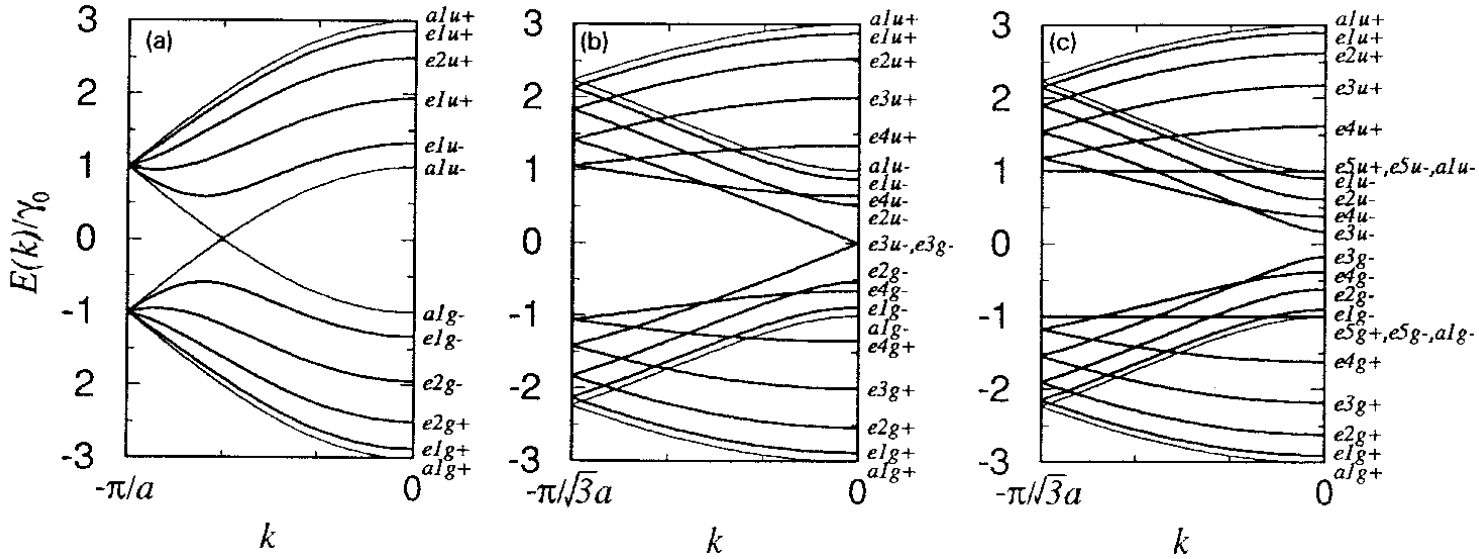

One-dimensional energy dispersion relations for (a) armchair (5,5) nanotubes, (b) zigzag (9,0) nanotubes and (c) zigzag (10,0) nanotubes.

Symmetry classification:

First letter (Mulliken symbol), names of the irreducible representations. *a*, *b* nondegenerate (one-dimensional), *e* two-fold degenerate (two-dimensional), *t* three-fold degenerate (three-dimensional). Often written as *A*, *B*, *E*, *T*
Subscripts 1, 2, 3 can be considered arbitrary labels.

g symmetric with respect to an inversion point (*u* antisymmetric).

Dresselhaus, Eklund, Adv. Phys. **49**, 705 (2000).

Van Hove peaks and resonant Raman spectroscopy

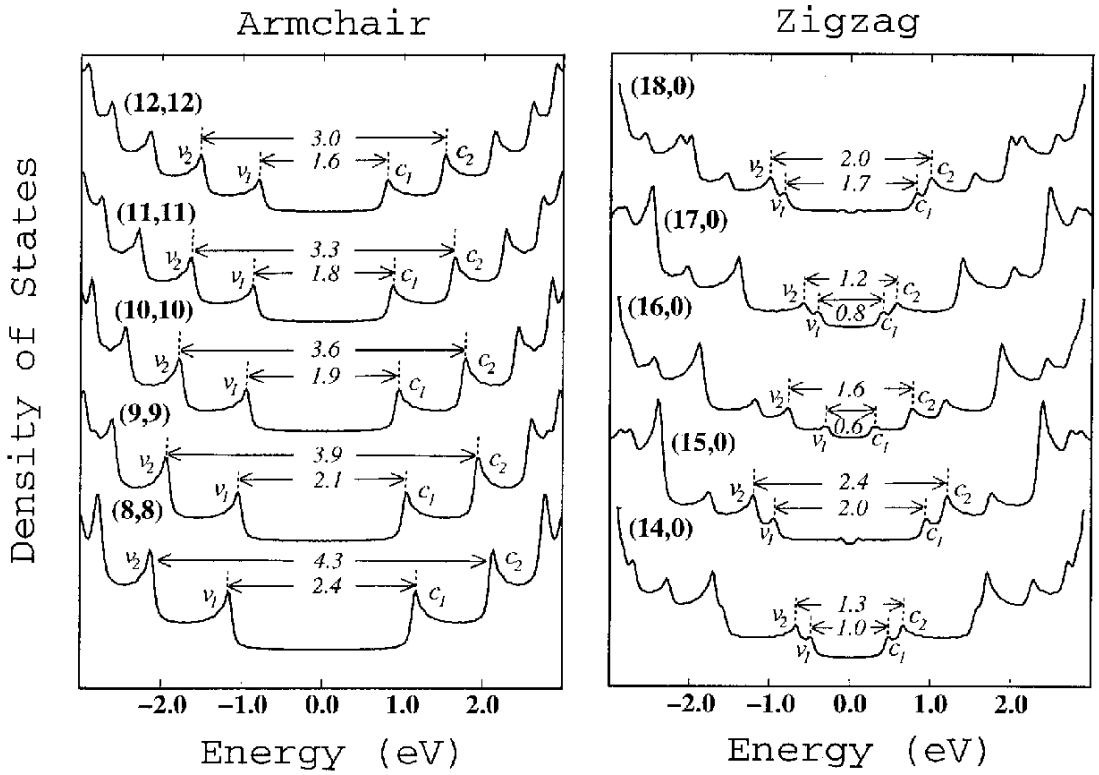

Electronic 1D density of states (DOS) calculated with a tight binding model for armchair and zigzag nanotubes and assuming a nearest neighbour carbon-carbon interaction energy $\gamma_0 = 3.0$ eV. Wavevector conserving optical transitions can occur between mirror image singularities in the 1D density of states, i.e. $\nu_1 \longrightarrow c_1$ and $\nu_2 \longrightarrow c_2$, etc. and these optical transitions are given in the figure in units of eV. These interband transitions are denoted by E_{11}, E_{22}, etc. and are responsible for the resonant Raman effect.

Calculating phonon spectra

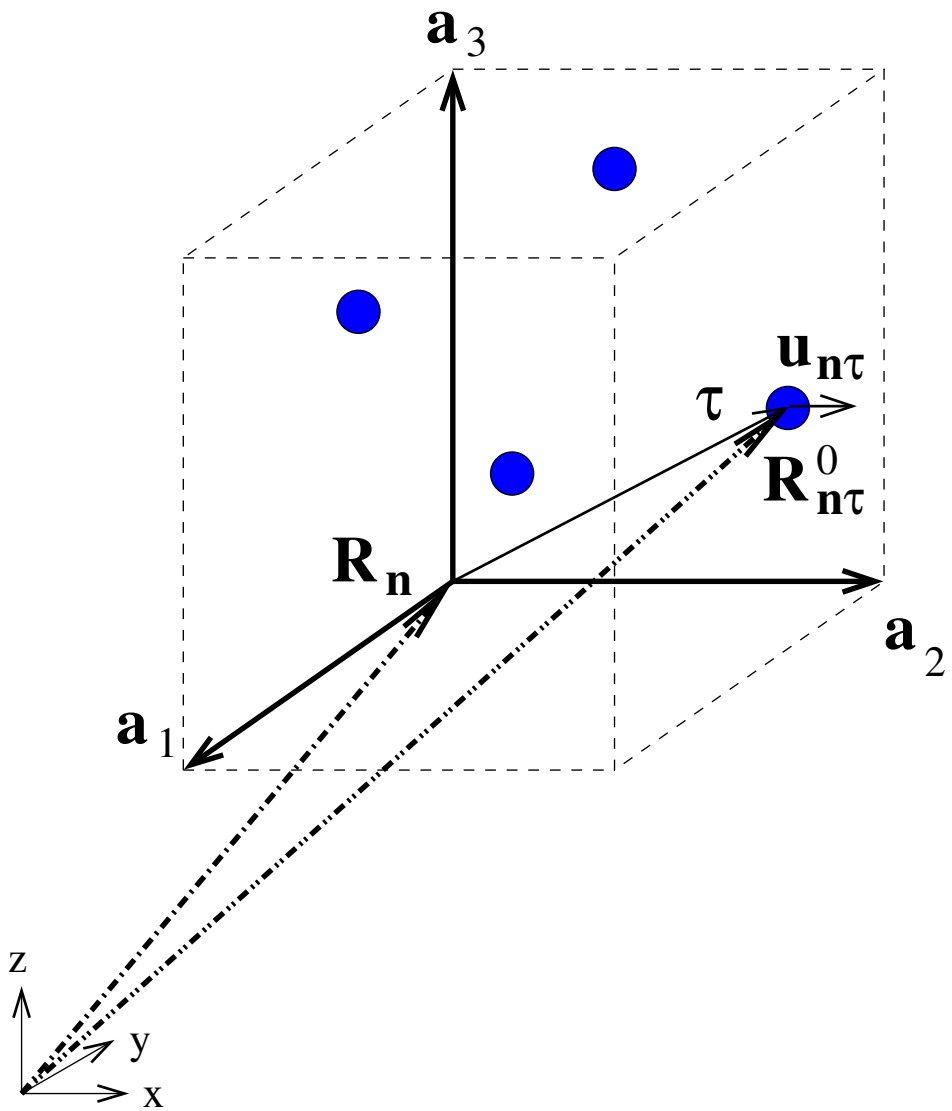

The Hamiltonian of the lattice in the ground state can be written as

$$\mathcal{H} = \mathcal{H}_{\text{ion}} + \mathcal{E}_{\text{el}} = \sum_{\mathbf{n}\tau} \frac{\mathbf{P}_{\mathbf{n}\tau}^2}{2M_\tau} + \mathcal{U}(\{\mathbf{R}_{\mathbf{n}\tau}\})$$

with the potential energy $\mathcal{U}$ depending on the positions of the atoms $\{\mathbf{R}_{\mathbf{n}\tau}\}$.

The integer vector $\mathbf{n} = (n_1, n_2, n_3)$ indicates the unit cell:

$\mathbf{R}_\mathbf{n} = n_1\mathbf{a}_1 + n_2\mathbf{a}_2 + n_3\mathbf{a}_3$.

τ points to the atoms in the unit cell forming the basis.

We now consider small displacements of the atoms from their equilibrium positions: $\mathbf{R}_{\mathbf{n}\tau}(t) = \mathbf{R}^0_{\mathbf{n}\tau} + \mathbf{u}_{\mathbf{n}\tau}(t)$

Calculating phonon spectra

Employing the widely used notation $u_{\mathbf{n}\tau i} = \begin{pmatrix} \mathbf{n} \\ \tau \\ i \end{pmatrix}$ (with i=1,2,3 indicating the Cartesian directions) we can expand the potential energy up to $\mathcal{O}(u^3)$

$$\mathcal{U}(\{\mathbf{R}_{\mathbf{n}\tau}\}) \approx \mathcal{U}(\{\mathbf{R}^0_{\mathbf{n}\tau}\}) + \sum_{\mathbf{n}\tau i} \Phi \begin{pmatrix} \mathbf{n} \\ \tau \\ i \end{pmatrix} u \begin{pmatrix} \mathbf{n} \\ \tau \\ i \end{pmatrix} + \frac{1}{2} \sum_{\substack{\mathbf{n}\tau i \\ \mathbf{m}\tau' j}} \Phi \begin{pmatrix} \mathbf{n} & \mathbf{m} \\ \tau & \tau' \\ i & j \end{pmatrix} u \begin{pmatrix} \mathbf{n} \\ \tau \\ i \end{pmatrix} u \begin{pmatrix} \mathbf{m} \\ \tau' \\ j \end{pmatrix}$$

with $\Phi \begin{pmatrix} \mathbf{n} \\ \tau \\ i \end{pmatrix} = \left. \frac{\partial \mathcal{U}}{\partial u_{\mathbf{n}\tau i}} \right|_{\{\mathbf{R}^0_{\mathbf{n}\tau}\}}$ and $\Phi \begin{pmatrix} \mathbf{n} & \mathbf{m} \\ \tau & \tau' \\ i & j \end{pmatrix} = \left. \frac{\partial^2 \mathcal{U}}{\partial u_{\mathbf{n}\tau i} u_{\mathbf{m}\tau' j}} \right|_{\{\mathbf{R}^0_{\mathbf{n}\tau}\}}$

In equilibrium, the first derivatives vanish, and considering only the second order terms defines the harmonic approximation with the Hamiltonian

$$\mathcal{H} = \sum_{\mathbf{n}\tau} \frac{\mathbf{P}^2_{\mathbf{n}\tau}}{2M_\tau} + \frac{1}{2} \sum_{\substack{\mathbf{n}\tau i \\ \mathbf{m}\tau' j}} \Phi \begin{pmatrix} \mathbf{n} & \mathbf{m} \\ \tau & \tau' \\ i & j \end{pmatrix} u \begin{pmatrix} \mathbf{n} \\ \tau \\ i \end{pmatrix} u \begin{pmatrix} \mathbf{m} \\ \tau' \\ j \end{pmatrix}$$

Calculating phonon spectra

Thus, the crystal is modeled as a system of masses M_τ connected by strings with force constants Φ. Newtons equations of motion are

$$M_\tau \ddot{u} \begin{pmatrix} \mathbf{n} \\ \tau \\ i \end{pmatrix} = - \sum_{\mathbf{m}\tau' j} \Phi \begin{pmatrix} \mathbf{n} & \mathbf{m} \\ \tau & \tau' \\ i & j \end{pmatrix} u \begin{pmatrix} \mathbf{m} \\ \tau' \\ j \end{pmatrix}$$

We can solve this system of coupled linear differential equations by writing

$$u_{\mathbf{n}\tau i}(t) = \frac{1}{\sqrt{M_\tau}} \bar{u} \begin{pmatrix} \mathbf{n} \\ \tau \\ i \end{pmatrix} e^{-i\omega t}$$

were a factor $1/\sqrt{M_\tau}$ is taken out of the displacement vector. This gives us a homogeneous system of coupled linear equations:

$$\omega^2 \bar{u} \begin{pmatrix} \mathbf{n} \\ \tau \\ i \end{pmatrix} = \sum_{\mathbf{m}\tau' j} \frac{1}{\sqrt{M_\tau M_{\tau'}}} \Phi \begin{pmatrix} \mathbf{n} & \mathbf{m} \\ \tau & \tau' \\ i & j \end{pmatrix} \bar{u} \begin{pmatrix} \mathbf{m} \\ \tau' \\ j \end{pmatrix}$$

Calculating phonon spectra

According to the Bloch theorem, displacements on different lattice sites differ only by phase factors:

$$\bar{u}\begin{pmatrix}\mathbf{n}\\ \tau\\ i\end{pmatrix} = \bar{u}\begin{pmatrix}0\\ \tau\\ i\end{pmatrix} e^{i\mathbf{q}\cdot\mathbf{R}^0_\mathbf{n}} = \bar{u}_{\tau i}(\mathbf{q}) e^{i\mathbf{q}\cdot\mathbf{R}^0_\mathbf{n}}$$

where the components of the wave vector are restricted to the discrete values

$$q_i = \frac{2\pi}{N_i a_i}\nu_i \qquad \nu_i = 0, \ldots, N_i - 1, \quad i = 1, 2, 3.$$

Thus, the coupled system of equations can be written as

$$\omega^2 \bar{u}_{\tau i}(\mathbf{q}) = \sum_{\tau' j} D_{\tau i, \tau' j}(\mathbf{q}) \bar{u}_{\tau' j}(\mathbf{q})$$

with the dynamical matrix

$$D_{\tau i, \tau' j}(\mathbf{q}) = \sum_{\mathbf{m}} \frac{1}{\sqrt{M_\tau M_{\tau'}}} \Phi \begin{pmatrix}\mathbf{n}-\mathbf{m} & 0\\ \tau & \tau'\\ i & j\end{pmatrix} e^{i\mathbf{q}\cdot(\mathbf{R}^0_\mathbf{m} - \mathbf{R}^0_\mathbf{n})}$$

Calculating phonon spectra

This is independent of $\mathbf{n}$, and $D_{\tau i,\tau' j}(\mathbf{q}) = D_{\tau i,\tau' j}(-\mathbf{q})$. The number of solutions to the coupled system of equations is equal to the number of the degrees of freedom $3rN$, with r atoms in the basis and N unit cells. For each $\mathbf{q}$ one has to solve the secular problem

$$\det\left(D_{\tau i,\tau' j}(\mathbf{q}) - \omega^2 \delta_{\tau\tau'}\delta ij\right) = 0$$

This gives $3r$ eigenfrequencies $\omega_s(\mathbf{q}) = \omega_s(-\mathbf{q}), s = 1, \ldots, 3r$ with corresponding normalized eigenvectors $\mathbf{e}^s_\tau(\mathbf{q})$. These frequencies correspond to collective modes of the crystal, and for one such collective mode $s\mathbf{q}$ the displacement of the ion at $\mathbf{R}_{\mathbf{n}\tau}$ is given by

$$\mathbf{u}^s_{\mathbf{n}\tau}(\mathbf{q}, t) \sim \frac{1}{\sqrt{M_\tau}} \mathbf{e}^s_\tau(\mathbf{q}) e^{i\left(\mathbf{q}\cdot\mathbf{R}^0_{\mathbf{n}} - \omega_s(\mathbf{q})t\right)}$$

The eigenvectors $\mathbf{e}^s_\tau(\mathbf{q})$ form a complete basis in which any movement of the individual ions can be expressed.

Phonon dispersion in graphite

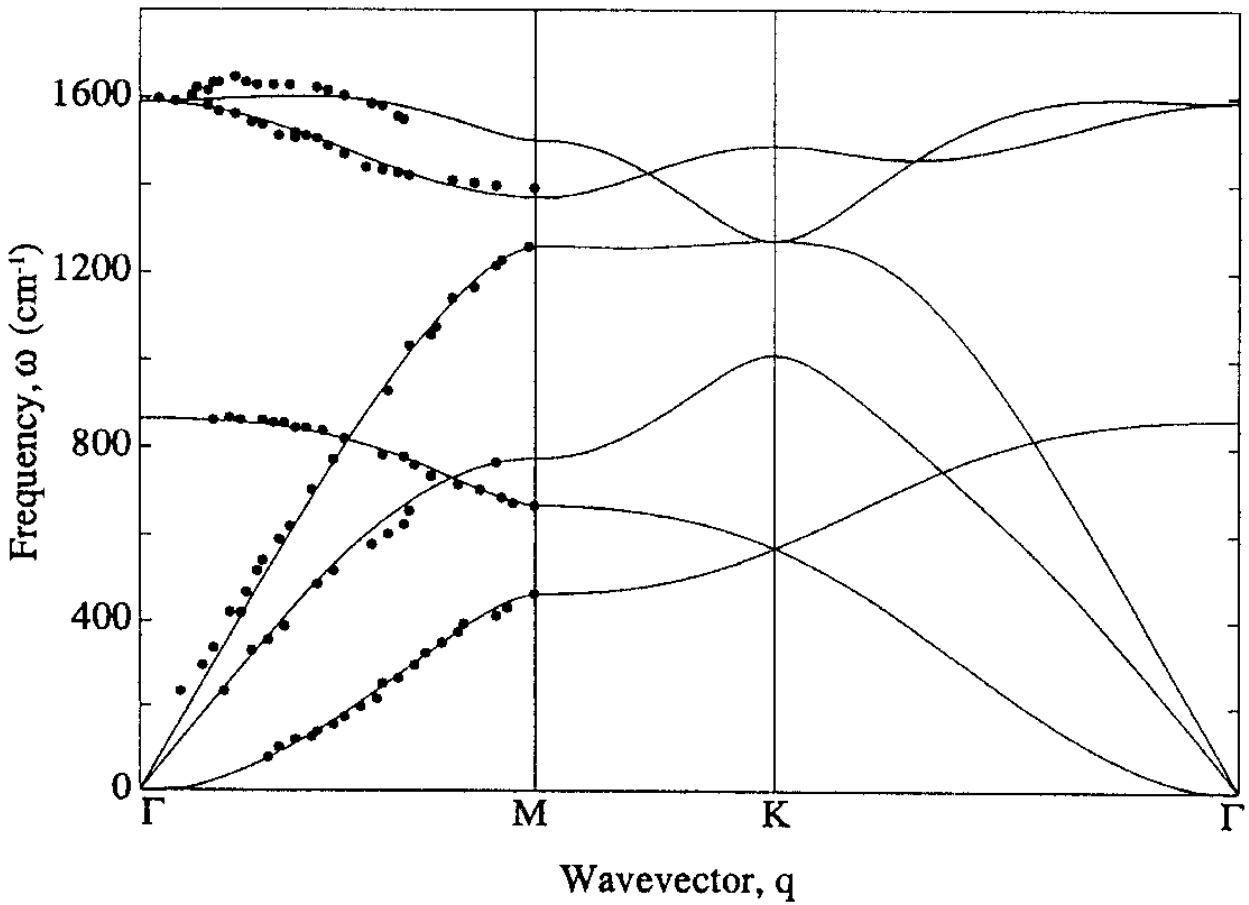

The phonon dispersion relations for graphite plotted along high-symmetry inplane directions. Experimental points from neutron scattering and electron energy loss spectra were used to obtain values for the force constants and to determine the phonon dispersion relations throughout the Brillouin zone.

Phonon dispersion of carbon nanotubes

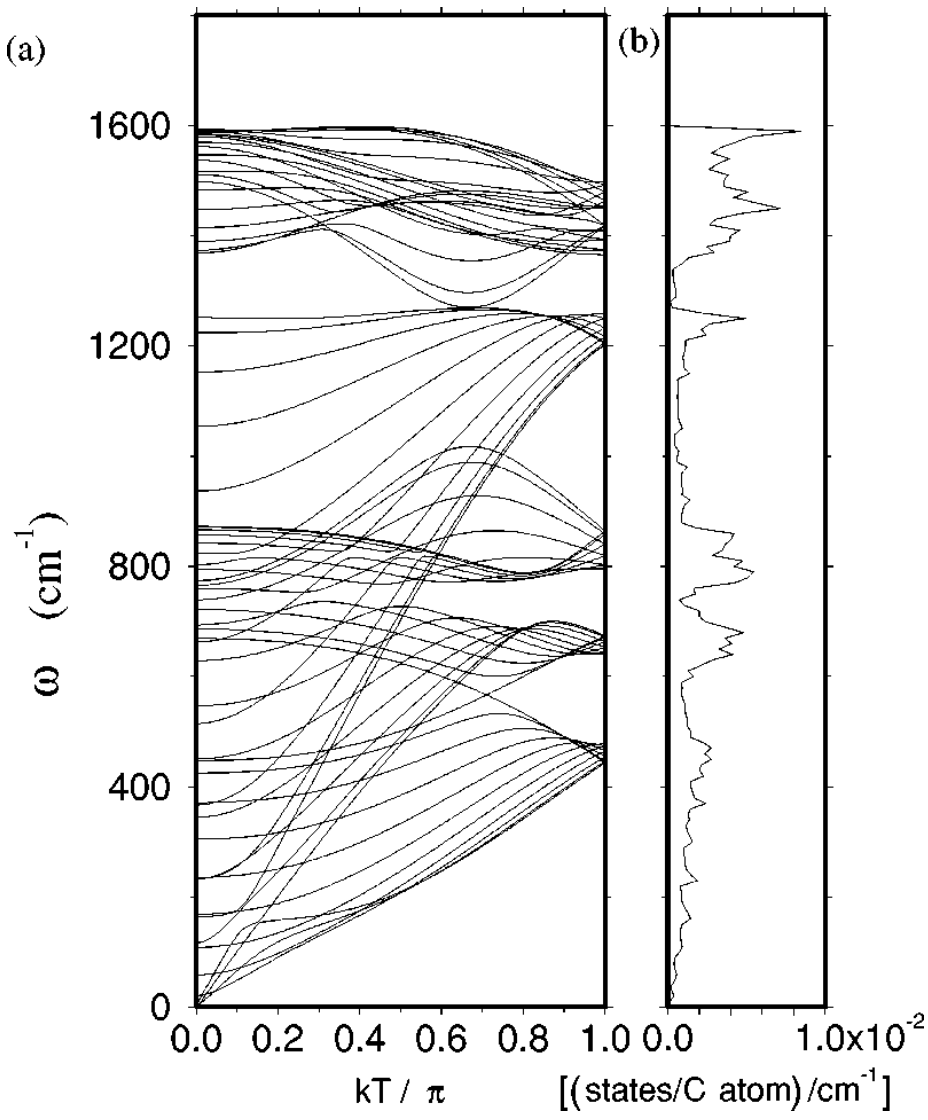

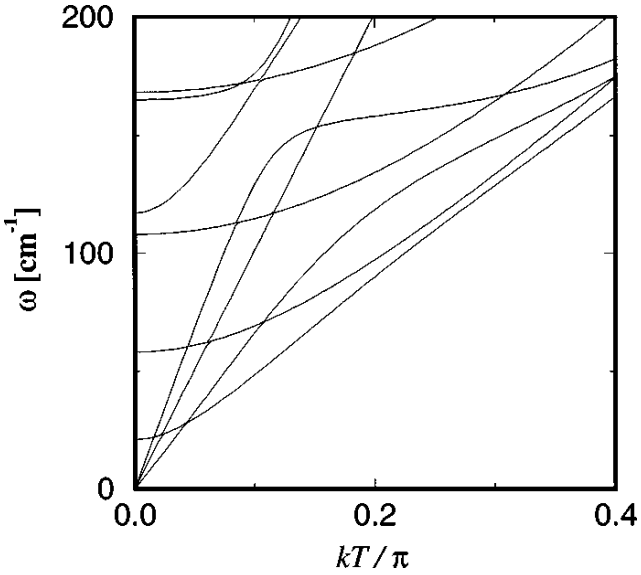

Left: Calculated phonon dispersion relations of a (10,10) armchair carbon nanotube. The number of degrees of freedom is 120, and the number of distinct phonon branches is 66. (b) Corresponding phonon density of states.

Right: Phonon dispersions of the same SWNT near the Γ point ($k = 0$).

Saito, Takeya, Kimura, Dresselhaus, Dresselhaus, Phys. Rev. B **57**, 4145 (1998).

Carbon nanotubes: Raman active phonon modes

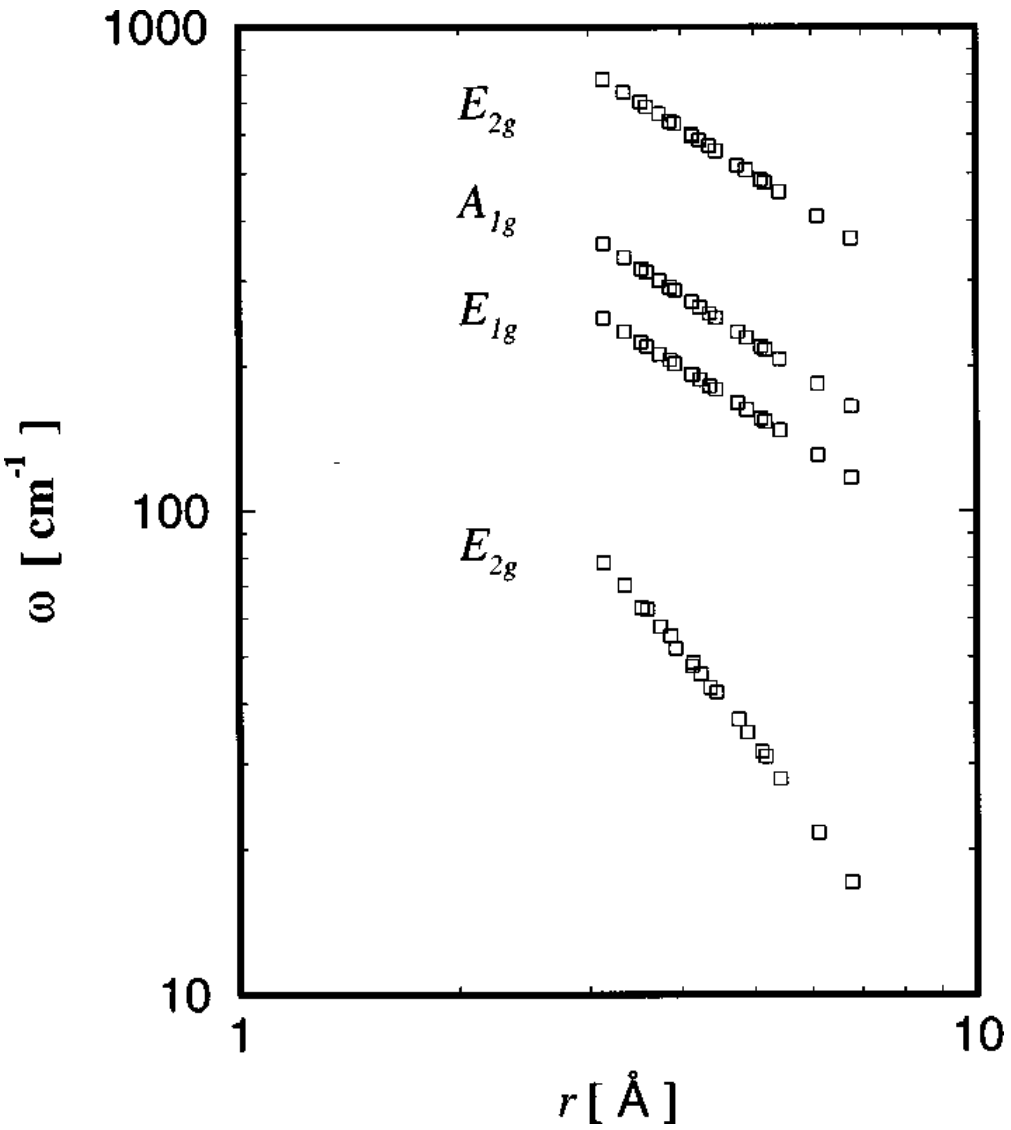

- Lowest lying Raman active mode is an E_{2g} mode in which the cross section of the CNT is vibrating with the symmetry described by the basis functions $x^2 - y^2$ and xy.
- Strongest low lying Raman active mode is the A_{1g} mode, which is the radial breathing mode (RBM). This mode provides a good marker for the CNT geometry as this mode is silent in graphite.

Carbon nanotubes: Raman active phonon modes

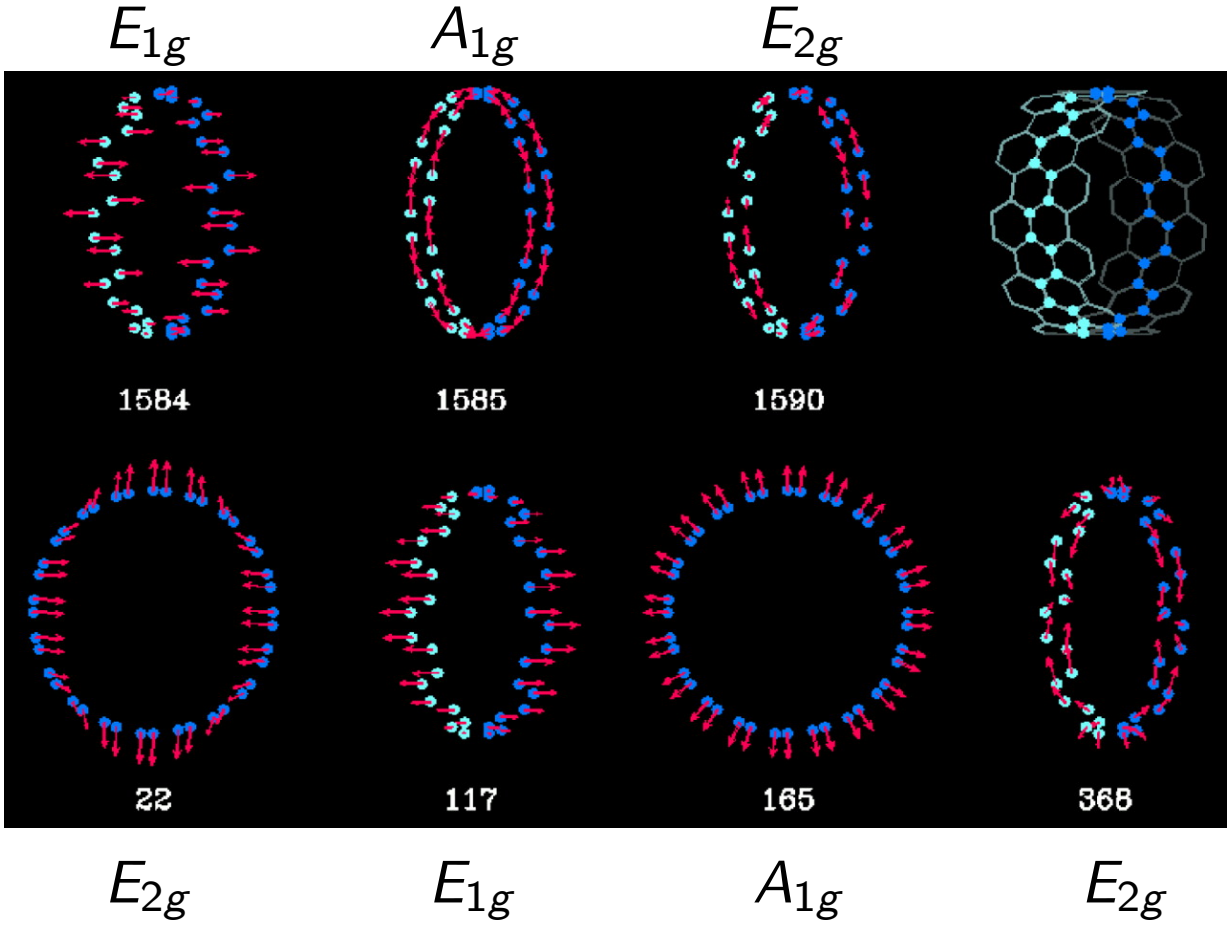

Raman-active normal mode eigenvectors and frequencies for a (10,10) nanotube. Red arrows indicate magnitude and direction of the appropriate C-atom displacements, and the eigenvectors shown correspond to the 7 most intense modes. The unit cell (blue atoms) is shown schematically in the upper right-hand corner.

Rao, Richter, Bandow, Chase, Eklund, Williams, Fang, Subbaswamy, Menon, Thess, Smalley, Dresselhaus, Dresselhaus, Science **275**, 187 (1997).

Carbon nanotubes: Raman spectroscopy

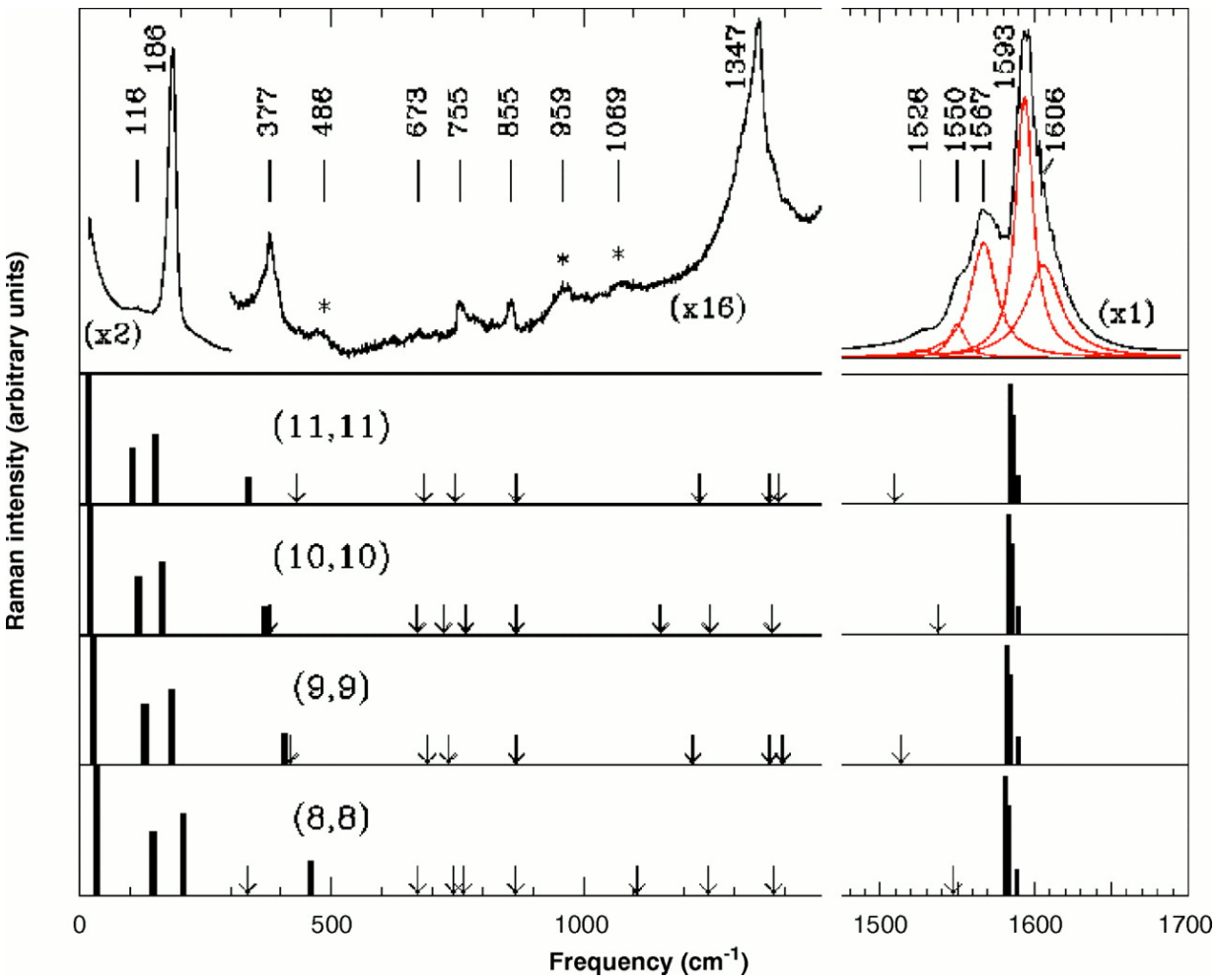

Raman spectrum (top) of SWNT samples taken with 514.5 nm excitation at ~ 2 W/cm^2. The four bottom panels are the calculated Raman spectra for armchair (n, n) nanotubes, $n = 8$ to 11. (Sample contains mainly these tubes). Downward pointing arrows in the lower panels indicate the positions of the remaining weak, Raman-active modes.

Introduction: Why study laser irradiation of carbon nanostructures theoretically?

- Carbon nanotubes can be produced in significant quantities (especially multiwall tubes).
- Grown nanotube ensembles are typically distributed over diameters and comprise many chiralities. They contain defects and even catalyst particles.
- But: Electronic properties depend crucially on geometry and perfection.

$\Rightarrow$ Efficient methods of CNT bundle manipulation are necessary! (Tips of scanning force microscopes are not enough).

Due to finely tunable parameters, a pulsed laser is a promising tool.

$\triangleright$ Theory can explore the possibilities!

Evolution of SWNT structure under laser irradiation

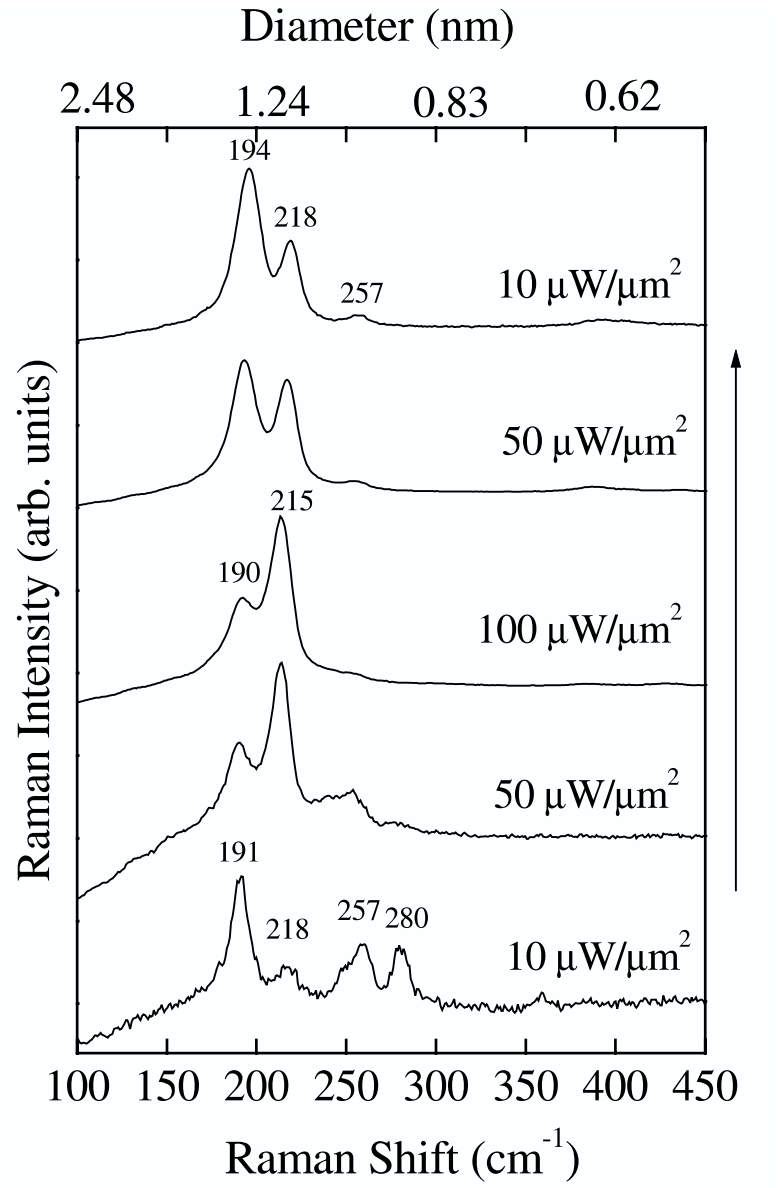

- Laser excitation of SWNT bundles at $\hbar\omega = 1.96$ eV, with intensity first increasing, then falling again.
- Observation of the radial breathing mode (RBM) frequency region. $\omega_{\mathrm{RBM}} = 248\mathrm{cm}^{-1}/d_t$, with d_t tube diameter in nm.

Corio, Santos, Pimenta, Dresselhaus, Chem. Phys. Lett. **360**, 557 (2002).

Evolution of SWNT structure under laser irradiation

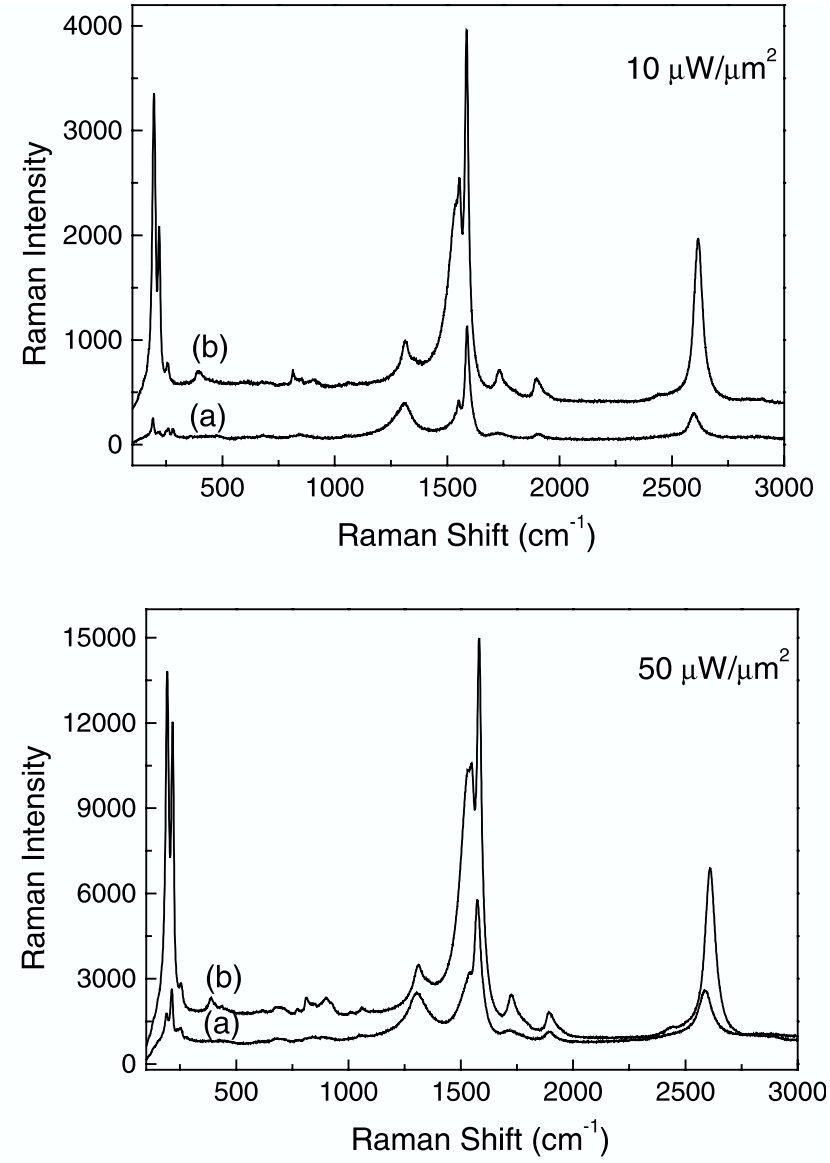

- Raman spectra before (a) and after (b) irradiation with 100 $\mu W/\mu m^2$ laser pulse; app. 10 times enhancement of intensity is observed.
- Possible explanation: Resonant Raman spectra depend strongly on sharp van Hove singularities in 1D DOS; but defects and disorder will broaden van Hove peaks. Thus, laser irradiation must have an annealing effect on SWNT bundle.

Euler-Lagrange equations of motion

- Mechanical system of f degrees of freedom described by $2f$ quantities. N particles have $3N$ degrees of freedom and are characterized by $6N$ quantities.
- Generalized coordinates $q_i = q_1, q_2, q_3, \ldots, q_f$ and generalized velocities $\dot{q}_i = \dot{q}_1, \dot{q}_2, \dot{q}_3, \ldots, \dot{q}_f$.
- Lagrangian of the system: $L = T(q_i, \dot{q}_i) - U(q_i)$.
- Hamilton's principle (action principle) demands, that the action $S = \int_{t_1}^{t_2} L(q_i, \dot{q}_i, t)dt$ between two configurations $\{q_i\}_1$ and $\{q_i\}_2$ at times t_1 and t_2 becomes extremal.
- Variation leads to Euler-Lagrange equations of motion: $\frac{d}{dt}\frac{\partial L}{\partial \dot{q}_i} - \frac{\partial L}{\partial q_i} = 0$
- Point particles $\longrightarrow$ Newton's equations of motion $m_i \ddot{q}_i = F_i$, but periodic boundary conditions are better treated in Lagrange formalism.

Periodic boundary conditions

- Coordinates $\mathbf{r}_i = h\mathbf{s}_i$ of atoms in primary MD unit cell are expressed by relative coordinates $\mathbf{s}_i$:

$$\mathbf{r}_i = \begin{pmatrix} a_x s_{ix} + b_x s_{iy} + c_x s_{iz} \\ a_y s_{ix} + b_y s_{iy} + c_y s_{iz} \\ a_z s_{ix} + b_z s_{iy} + c_z s_{iz} \end{pmatrix}$$

$$= s_{ix}\mathbf{a} + s_{iy}\mathbf{b} + s_{iz}\mathbf{c}.$$

- Lagrangian (with T for transposition):

$$L = \sum_{i=1}^{N} \frac{m_i}{2} \dot{\mathbf{s}}_i^{\mathrm{T}} h^{\mathrm{T}} h \dot{\mathbf{s}}_i - U(\{r_{ij}\}).$$

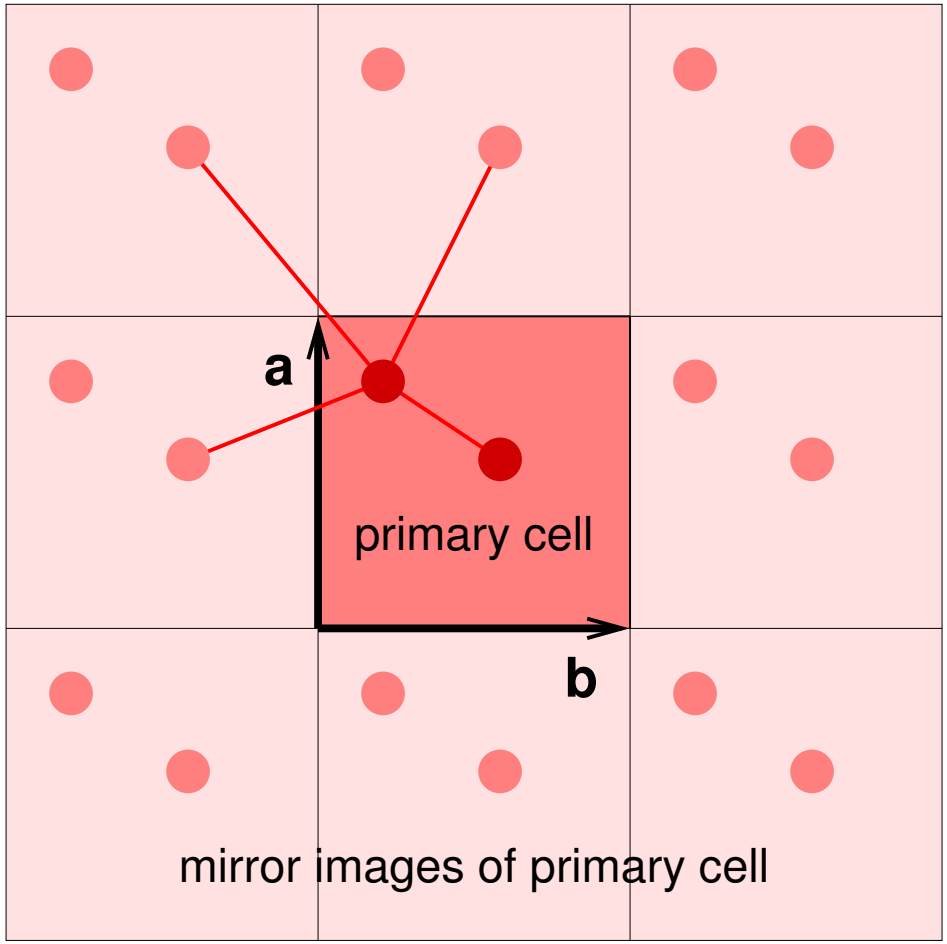

Choice of interaction potential

Force field methods

- Parametrized potentials for the interaction between 2, 3 or more atoms.
- Can treat millions of atoms.
- Knows nothing of electrons (chemistry, laser excitation).

Tight binding molecular dynamics

- Parametrization of overlap integral of atomic wave functions.
- Can treat one thousand atoms.
- Chemistry described decently, laser with additional equations.

Ab initio molecular dynamics

- Quantum mechanical description.
- Can treat two hundred atoms.
- Chemistry described very well, laser not so simple.

Verlet algorithm

- Taylor expansion for the coordinate $r_{i\alpha}$ (lattice site i, $\alpha \in \{x, y, z\}$) at time $t + \tau$ and $t - \tau$:

$$r_{i\alpha}(t+\tau) = r_{i\alpha}(t) + \tau \frac{dr_{i\alpha}(t)}{dt} + \frac{\tau^2}{2} \frac{d^2 r_{i\alpha}(t)}{dt^2} + \frac{\tau^3}{3!} \frac{d^3 r_{i\alpha}(t)}{dt^3} + O(\tau^4),$$

$$r_{i\alpha}(t-\tau) = r_{i\alpha}(t) - \tau \frac{dr_{i\alpha}(t)}{dt} + \frac{\tau^2}{2} \frac{d^2 r_{i\alpha}(t)}{dt^2} - \frac{\tau^3}{3!} \frac{d^3 r_{i\alpha}(t)}{dt^3} + O(\tau^4).$$

- When adding these Eqs., only even derivatives remain:

$$r_{i\alpha}(t+\tau) = 2r_{i\alpha}(t) - r_{i\alpha}(t-\tau) + \tau^2 \frac{d^2 r_{i\alpha}(t)}{dt^2} + O(\tau^4).$$

- Subtraction yields for the velocities:

$$\frac{dr_{i\alpha}(t)}{dt} = \frac{1}{2\tau} \left[r_{i\alpha}(t+\tau) - r_{i\alpha}(t-\tau) \right] + O(\tau^3).$$

- These equations are called Verlet algorithm.

Workflow of a molecular dynamics simulation

0. The initial state of a system is established by choosing the coordinates $\mathbf{r}_i(t)$ of all particles and of their velocities $\dot{\mathbf{r}}_i(t)$ at start time $t = 0$.

---

1. From the distances $r_{ij} = |\mathbf{r}_i - \mathbf{r}_j|$ the interaction potential $U(\{r_{ij}\})$ is calculated.
2. The forces acting on all particles are determined as gradients of the potential: $\mathbf{F}_i = \nabla_i U(\{r_{ij}\})$
3. By applying the Verlet algorithm to all coordinates and velocities new positions $\mathbf{r}_i(t+\tau)$ and velocities $\dot{\mathbf{r}}_i(t+\tau)$ at time $t+\tau$ are obtained.

---

4. Molecular dynamics simulation: Iteration of steps 1 (new potential), 2 (new forces), and 3 (new positions and velocities).

Tight binding molecular dynamics

Molecular dynamics (MD) based on Lagrange function (Andersen 1980, Parrinello, Rahman 1980)

$$L(t) = \sum_{i=1}^{N} \frac{m_i}{2} \dot{\mathbf{s}}_i^{\mathrm{T}} h^{\mathrm{T}} h \dot{\mathbf{s}}_i + K_{cell} - U(\{r_{ij}\}, t) - P\Omega \,,$$

$\mathbf{s}_i \equiv$ relative coordinates; MD unit cell spanned by $\mathbf{a}$, $\mathbf{b}$ and $\mathbf{c}$, (3×3) matrix $h = (\mathbf{a}\ \mathbf{b}\ \mathbf{c}) \Rightarrow \mathbf{r}_i = h\mathbf{s}_i$, $r_{ij} = |\mathbf{r}_i - \mathbf{r}_j|$.
$K_{cell} \equiv$ kinetic energy of MD unit cell,
$U(\{r_{ij}\}, t) \equiv$ interaction potential.

$\Rightarrow$ **Equations of motion** for coordinates $\mathbf{s}_i$ and unit cell h_{kl}.

Interatomic interaction potential

$$U(\{r_{ij}\}, t) = \sum_m n(\epsilon_m, t)\, \epsilon_m + \Phi_{rep}(\{r_{ij}\}) \,,$$

$\Phi_{rep} \equiv$ ion ion repulsion; $\epsilon_m = \langle m | H_{\mathrm{TB}} | m \rangle \equiv$ eigenvalues of the tight binding Hamiltonian $H_{\mathrm{TB}} = \sum_{i\alpha} \epsilon_{i\alpha} n_{i\alpha} + \sum_{\substack{ij\alpha\beta \\ j \neq i}} t_{ij}^{\alpha\beta} c_{i\alpha}^{+} c_{j\beta}$,

Beyond tight binding molecular dynamics

$n(\epsilon_m, t) \equiv$ occupation of electronic energy levels
(dependence on time is nonstandard!).

$\Rightarrow$ **Forces:** $\mathbf{F}_i = -\frac{\partial U(\{r_{ij}\},t)}{\partial \mathbf{s}_i}$ and $\mathbf{F}_{\alpha\beta} = -\frac{\partial U(\{r_{ij}\},t)}{\partial h_{\alpha\beta}}$ (unit cell deformation; in nanotubes: longitudinal expansion and contraction).

Electron dynamics in nonequilibrium:

$$\frac{dn(\epsilon_m,t)}{dt} = \int_{-\infty}^{\infty} d\omega\, g(\omega,t)\Big\{ n(\epsilon_m-\hbar\omega,t) + n(\epsilon_m+\hbar\omega,t) - 2n(\epsilon_m,t)\Big\} - \frac{n(\epsilon_m,t)-n^0(\epsilon_m,T_{el})}{\tau_1}$$

$g(\omega, t) \equiv$ spectral distribution of laser pulse (pulse envelope, color).
$\epsilon_m \to \epsilon_m \pm \hbar\omega$. $\tau_1 \equiv$ thermalization time of electrons

In equilibrium: $n = n^0(\epsilon_m, T_{el}) = \left[\exp\{\frac{\epsilon_m-\mu}{k_B T_{el}}\}+1\right]^{-1}$ Fermi function, with electron temperature $T_{el}(t)$.

Destruction of CNT at high energies

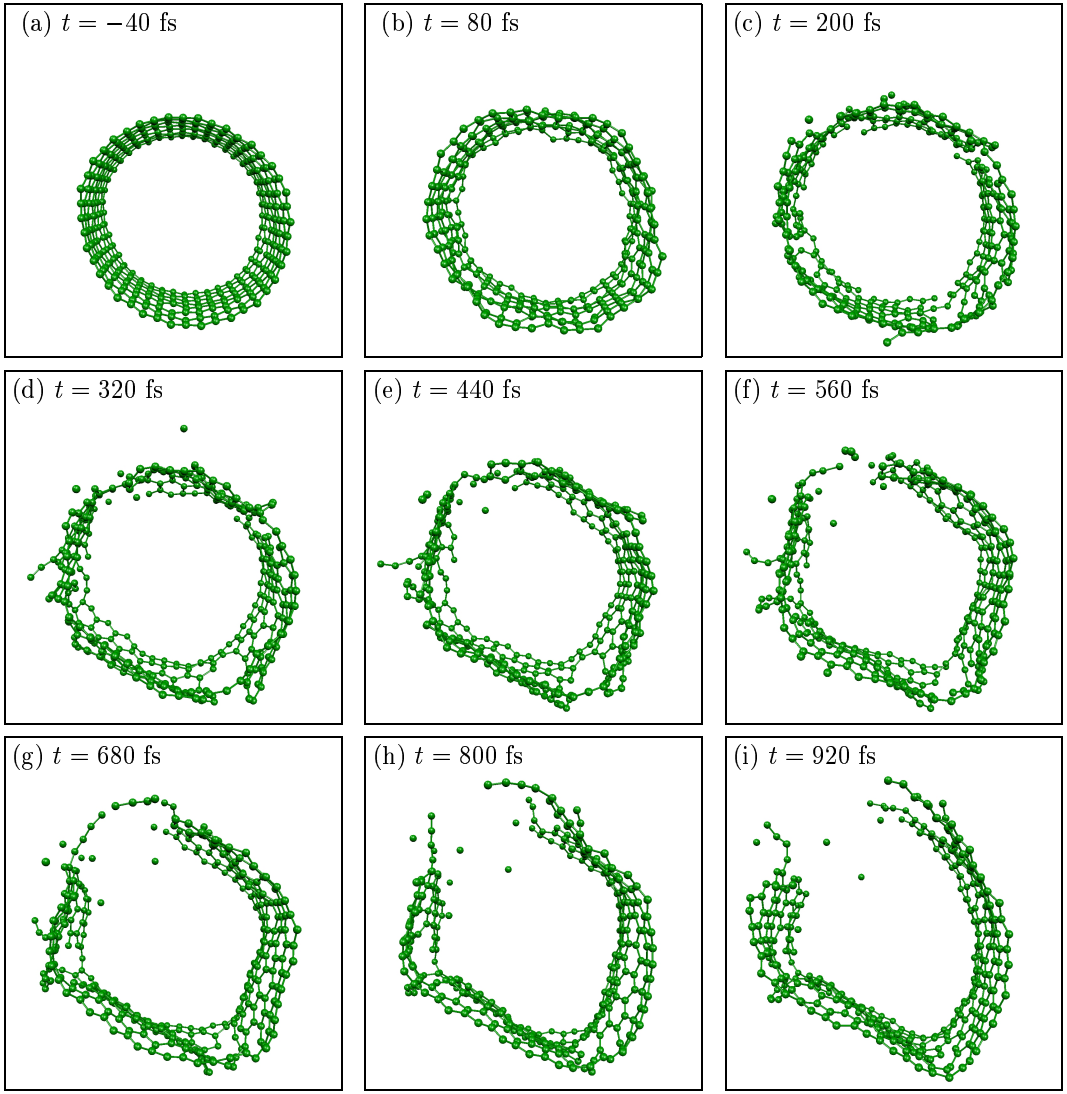

- View along a (22,0) single wall nanotube.
- Periodic boundary conditions make this tube infinite in length.
- Laser pulse of $\tau = 20$ fs duration acts at time $t = 0$.
- Laser intensity 30% above damage threshold.
- Energy suffices for **massive bond breaking** and destruction of CNT wall.

CNT damage slightly above threshold

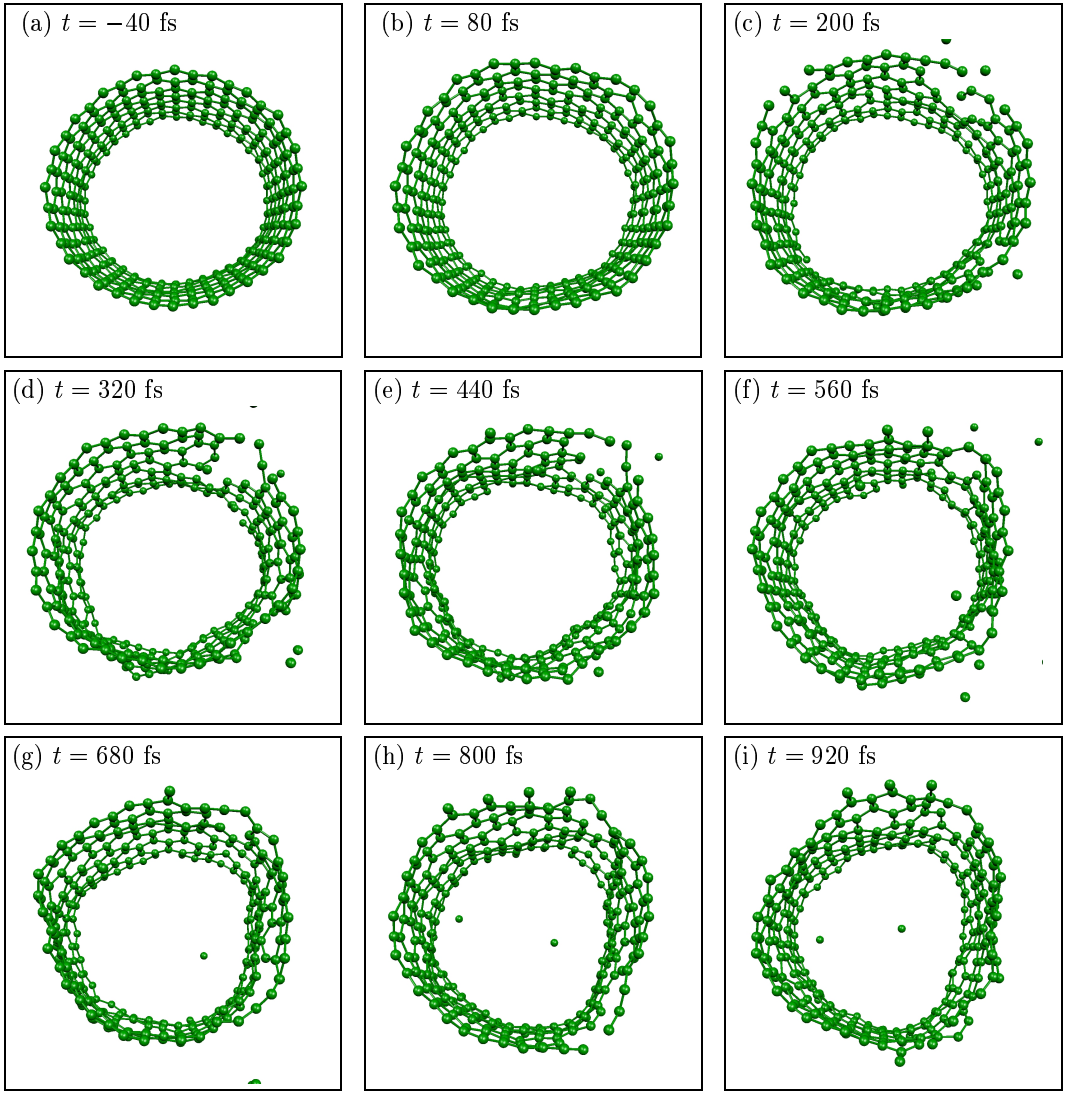

- View along a (20,0) single wall nanotube.
- Laser pulse of $\tau = 20$ fs duration with an intensity of only 8% above the damage threshold.
- CNT is damaged by emission of carbon atoms or small clusters.

Strong vibrational excitation slightly below threshold

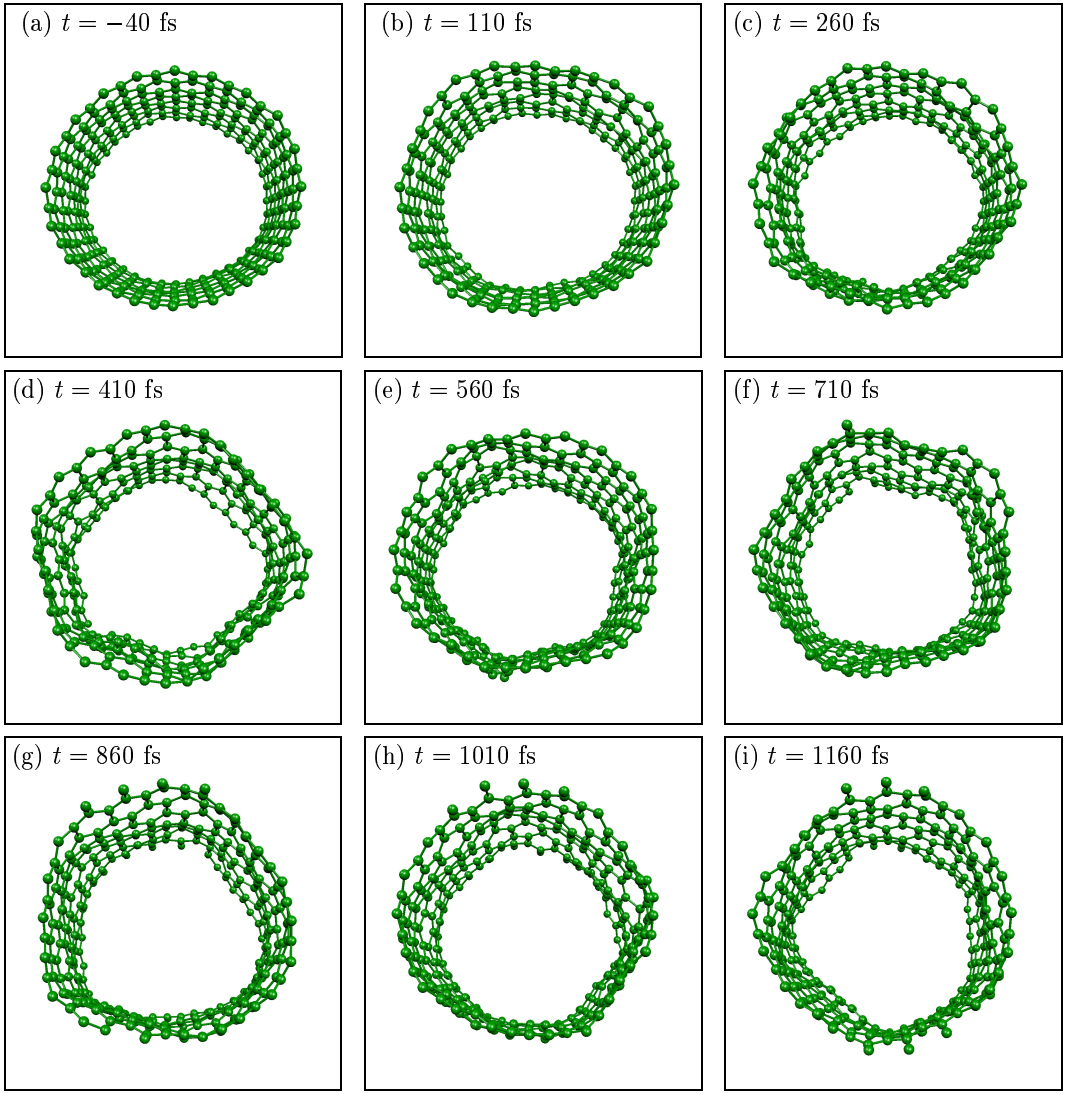

- View along a (20,0) single wall nanotube.
- Laser pulse of $\tau = 20$ fs duration with an intensity 4% below the damage threshold.
- SWNT wall stays intact (no bond breaking) but shows strong oscillations.
- ▷ What is the nature of these vibrations?

Analysis of SWNT vibrational excitation

Plan: cut up $(22, 0)$ CNT into eight 44 atom sections, fit coordinates to nearest circle by minimizing the function $f(x_0, y_0, r) = \sum_{i=1}^{N_{\text{slab}}} \left(\sqrt{(x_i - x_0)^2 + (y_i - y_0)^2} - r \right)^2$

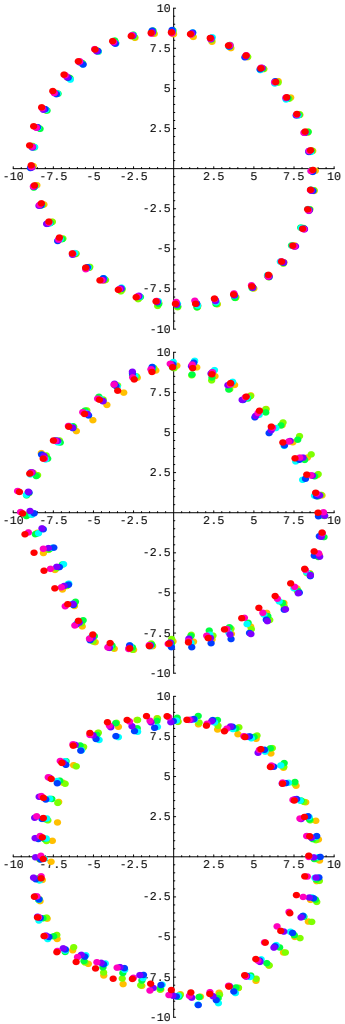

Projected slabs: Time

$t = 0$ ps

$t = 0.9$ ps

$t = 1.9$ ps

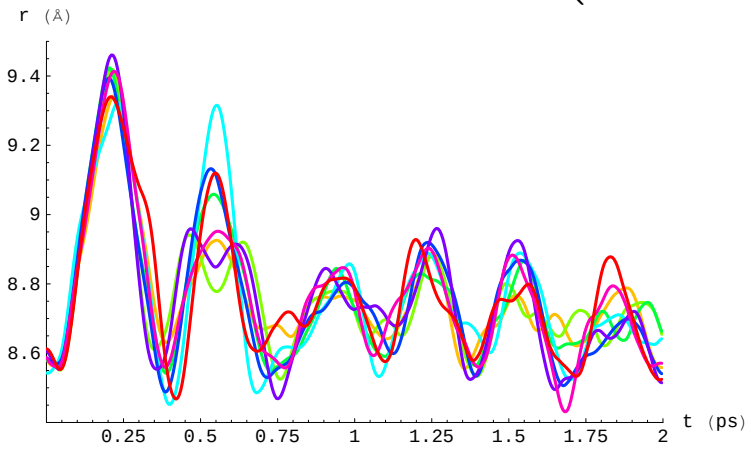

Radial breathing mode: *Coherent oscillations of section radii*

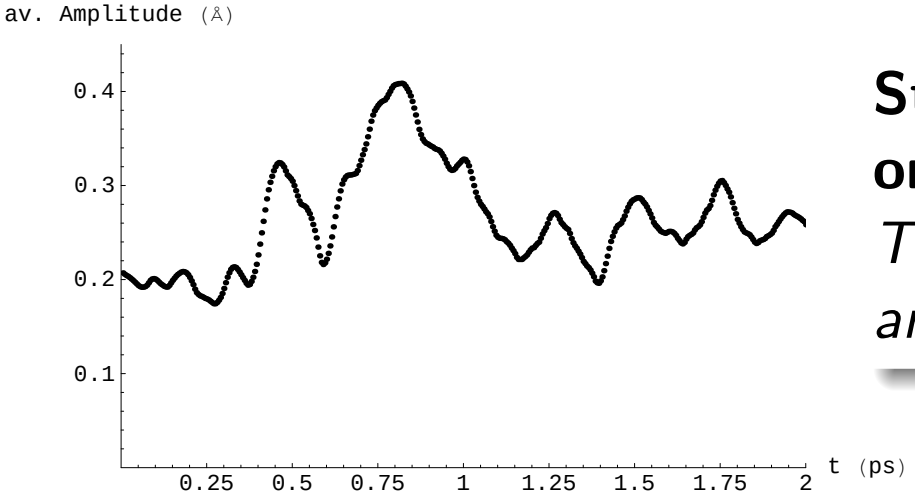

Standing wave on CNT wall: *Time evolution of amplitude*

Zigzag SWNT damage thresholds as a function of diameter

Thresholds for pulse duration $\tau = 20$ fs, frequency $\hbar\omega = 1.96$ eV, given in absorbed energy E_0 per atom, extracted from many trajectories:

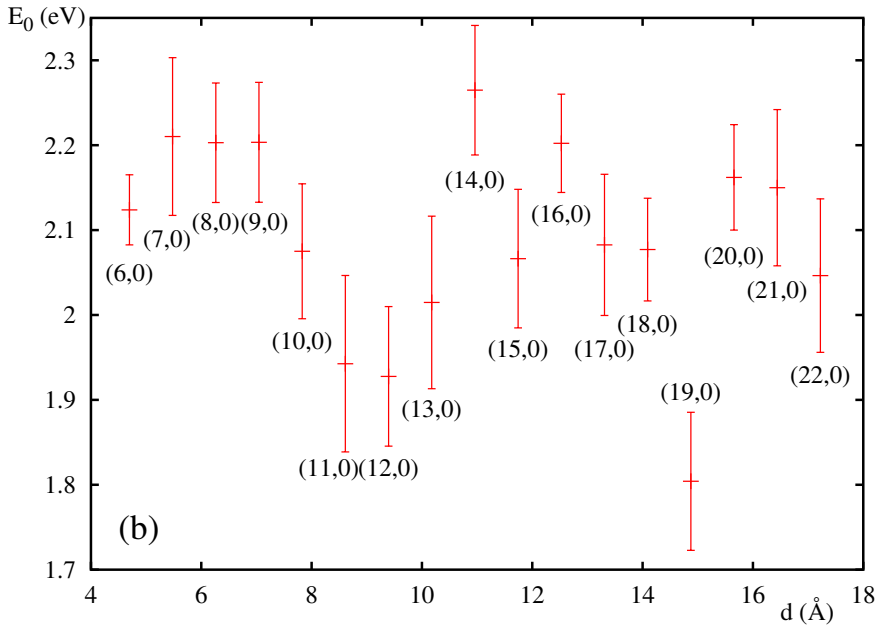

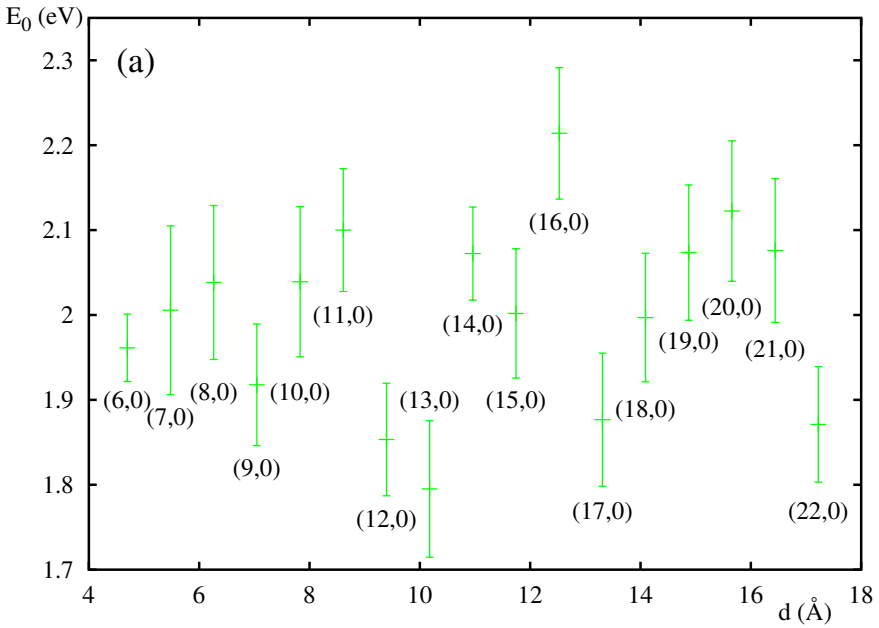

- *Bondary conditions allow longitudinal expansion*

- *Bondary conditions suppress longitudinal expansion*

- Possibility of longitudinal expansion leads to higher stability
- **Nonmonotonous diameter dependence of stability**

Armchair SWNT damage thresholds

Diameter and boundary condition dependence

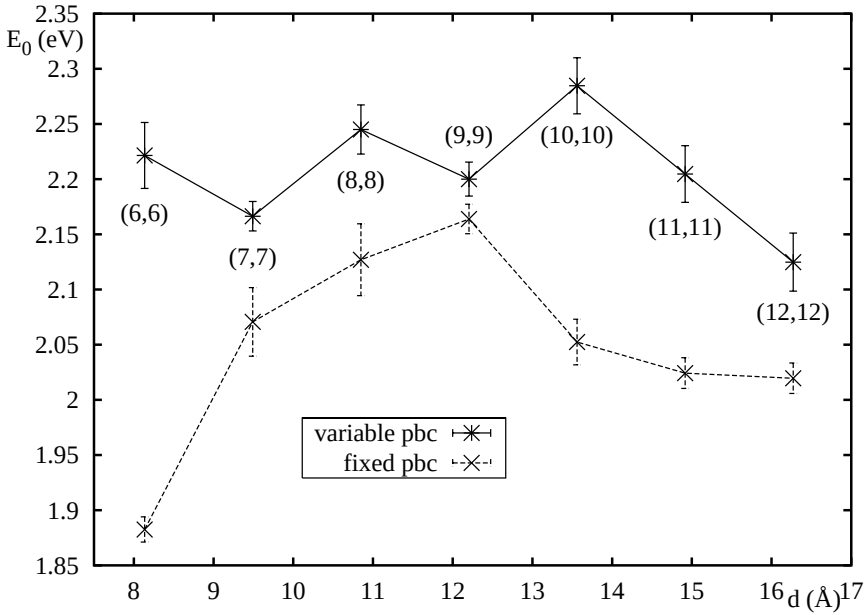

- Observations similar to zigzag CNTs:
  - Stability maximum at $d \approx 12$ Å
  - Longitudinal expansion increases stability

Diameter and pulse duration dependence

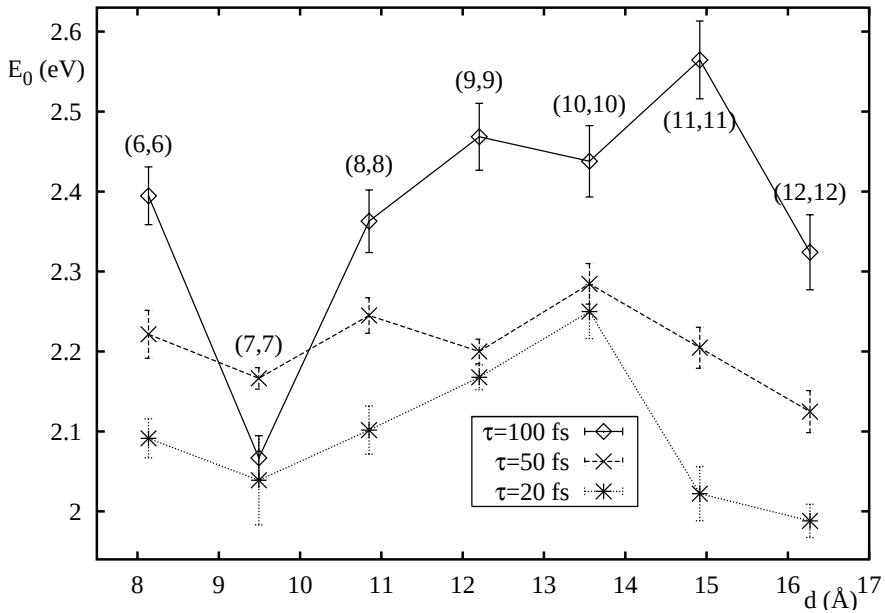

- Stability increases with pulse duration! Energy has more time to distribute over degrees of freedom during longer pulse.

Thermal↔nonthermal nanodiamond to fullerene transition

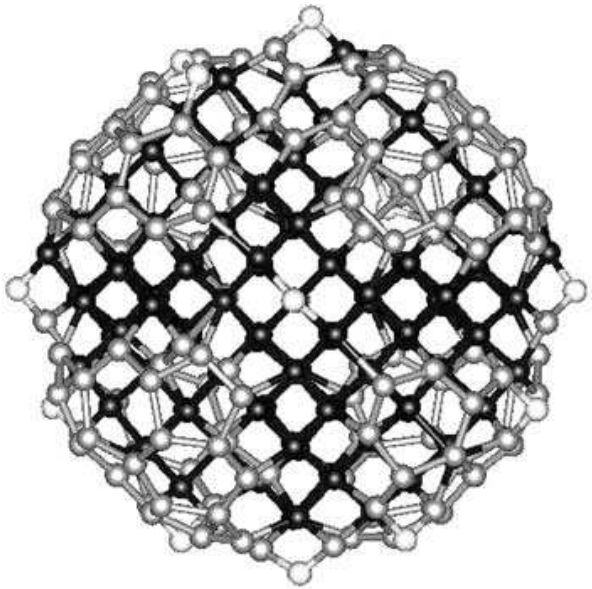

$\tau = 50$ fs laser pulse

Annealing at $T = 2000$ K

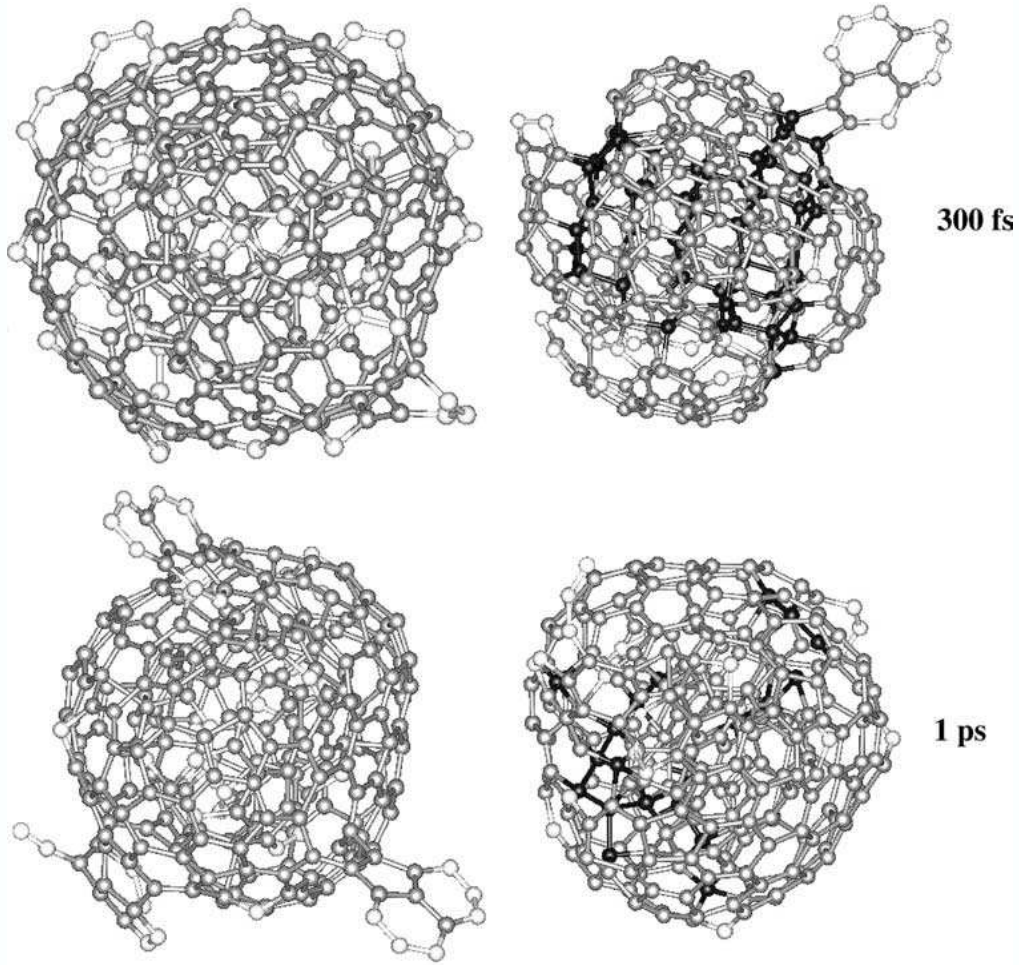

- Nanodiamond prepared by *ab initio* structure optimization and TBMD annealing.
- Gray scale coding of hybridization:
  Black atoms/bonds $\equiv sp^3$,
  gray atoms/bonds $\equiv sp^2$.

Laser enhances sp^3 to sp^2 transition

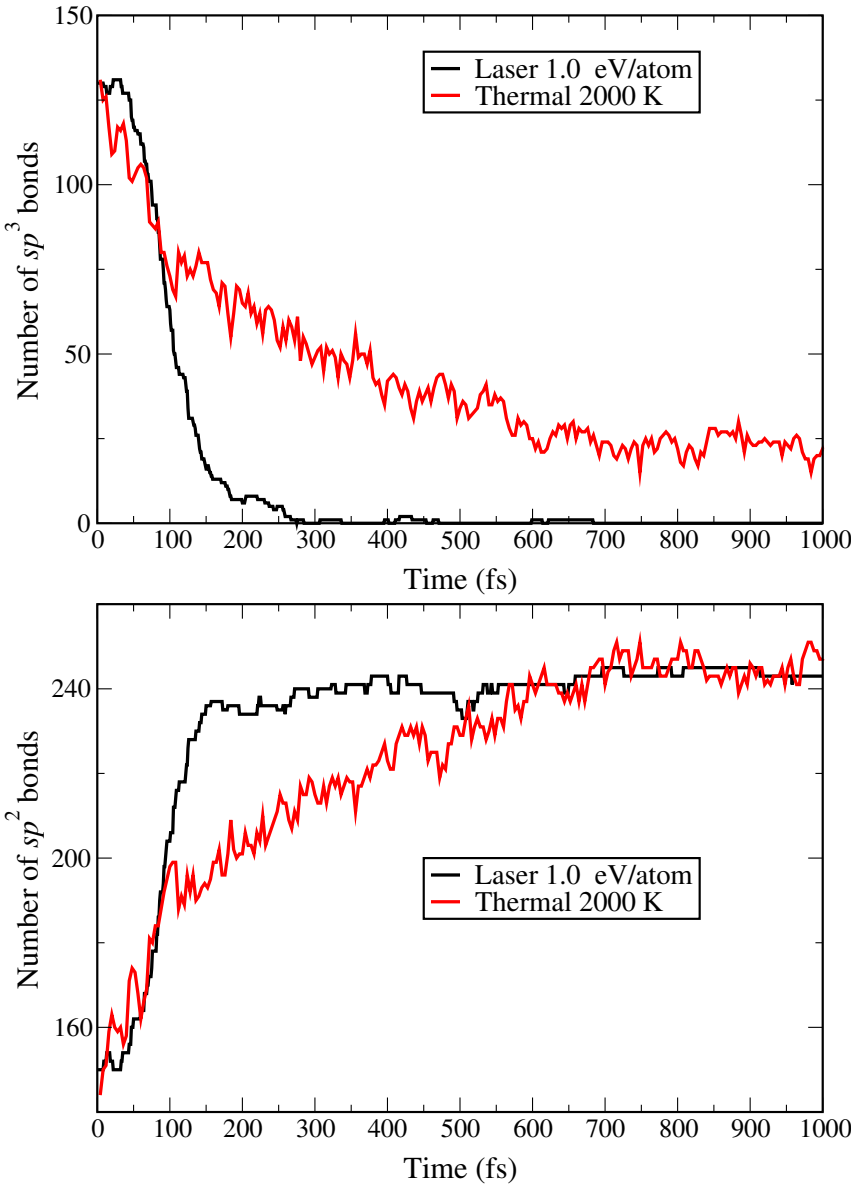

- Comparison of sp^3 bond breaking and sp^2 bond formation for thermal and nonthermal cases.
- Laser transition to fullerene-like structure is faster and more complete.
- Due to strong radial breathing mode induced by laser irradiation, sp^2 bond formation proceeds from the cluster core to the surface.
- Thermal sp^2 bond formation, in contrast, starts at the cluster surface.

$\longrightarrow$ Should be investigated further.

Electronic temperature and capped nanotube structure

- Color coding of structure: C-C bond length colors range from blue for $d_{C-C} < 1.4$ Å to red for $d_{C-C} > 1.52$ Å.
- Structure at constant elevated electron temperature of $T_e = 25000$ K shows significant bond expansion/weakening.
- Bond elongation, *i.e.* strain, is higher in caps.

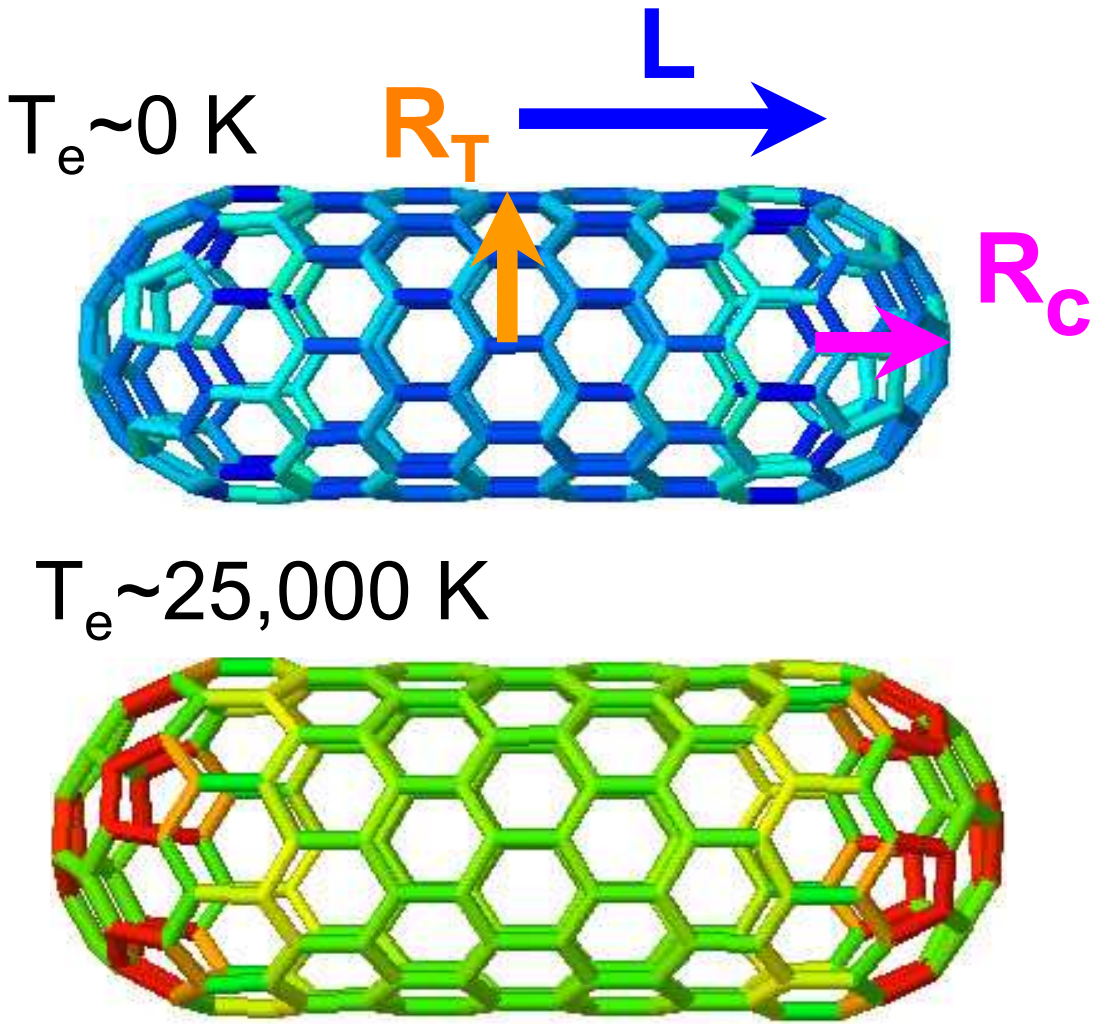

Below threshold laser excitation of capped nanotube

- $(10, 0)$ CNT response to $\tau = 10$ fs pulse, 15% below damage threshold

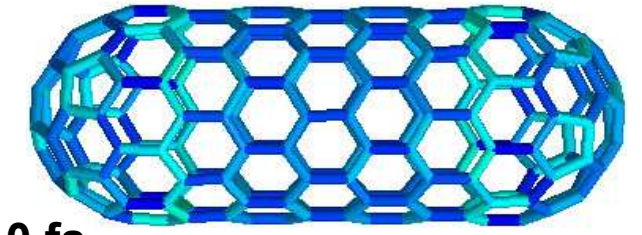

0 fs

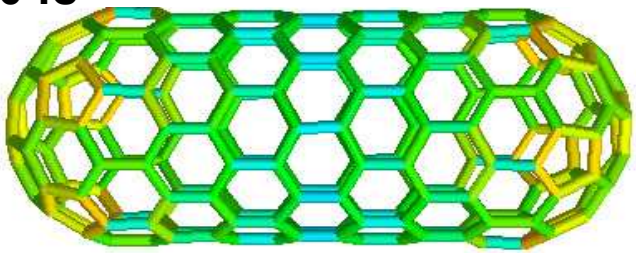

50 fs

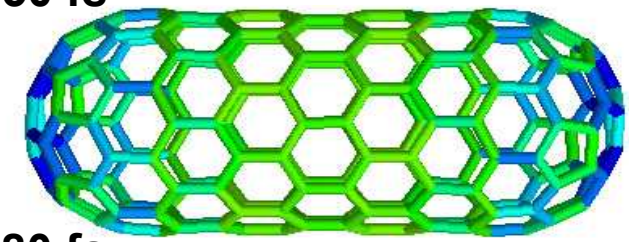

80 fs

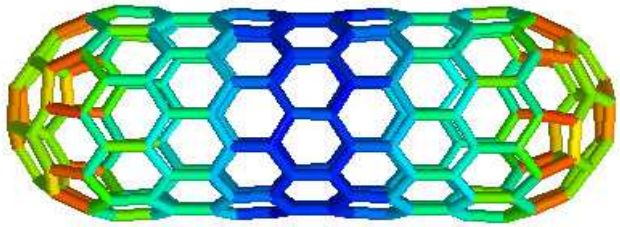

120 fs

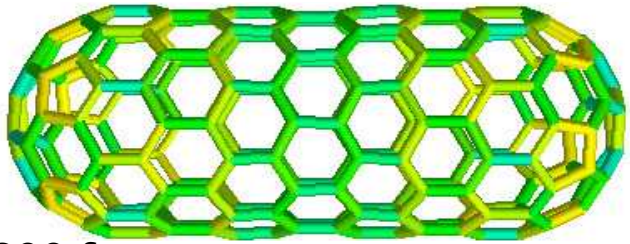

200 fs

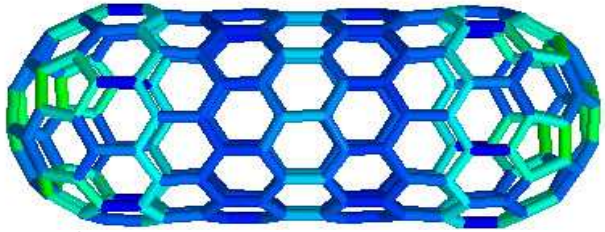

250 fs

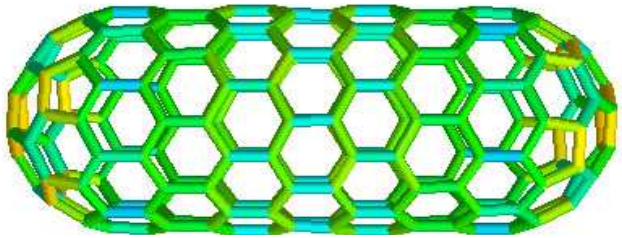

300 fs

Laser excited capped CNTs: Identification of coherent phonons

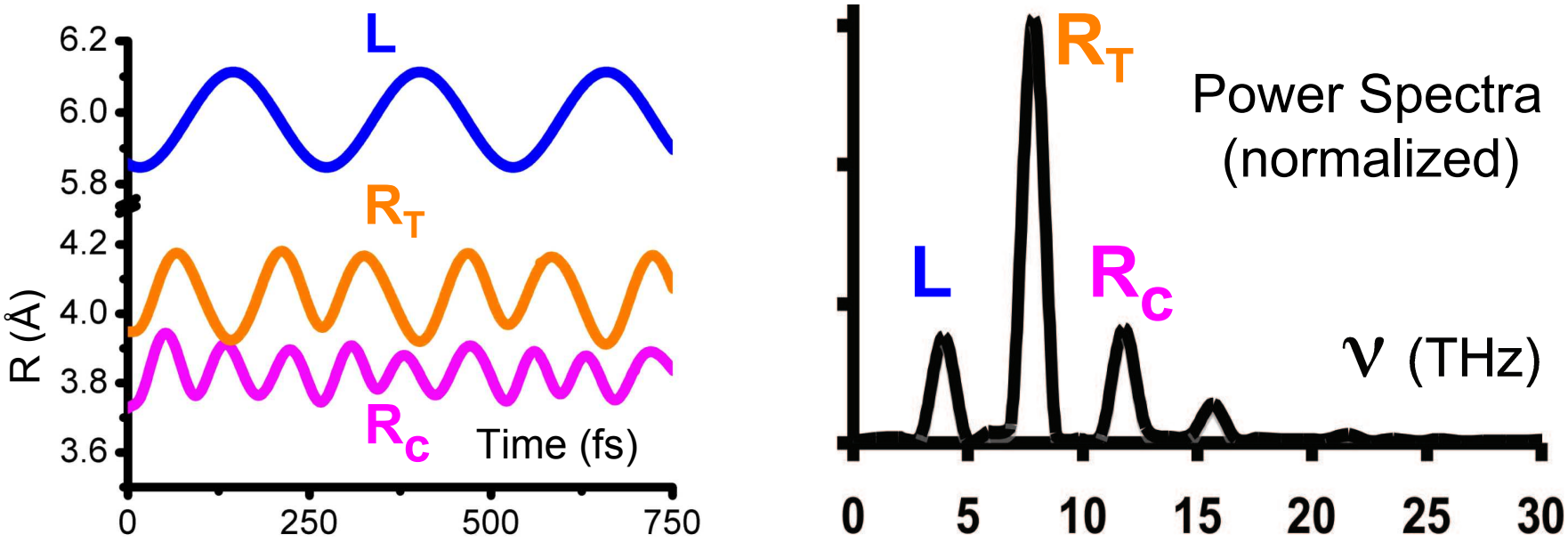

- Identification of a longitudinal breathing mode in the tube body (L), a transversal mode of the body (R_T) or radial breathing mode (RBM) and a breathing mode of the cap (R_C).
- These modes can be extracted by averaging over the coordinates (left) and by Fourier transforming the velocity autocorrelation function (right).

Laser induced cap opening: Mechanism

- Simultaneous excitation of coherent phonons with different periods.
- Strain maximum when cap and body breathing modes are of opposite phase.

⇒ **Clean separation of tube and body!**

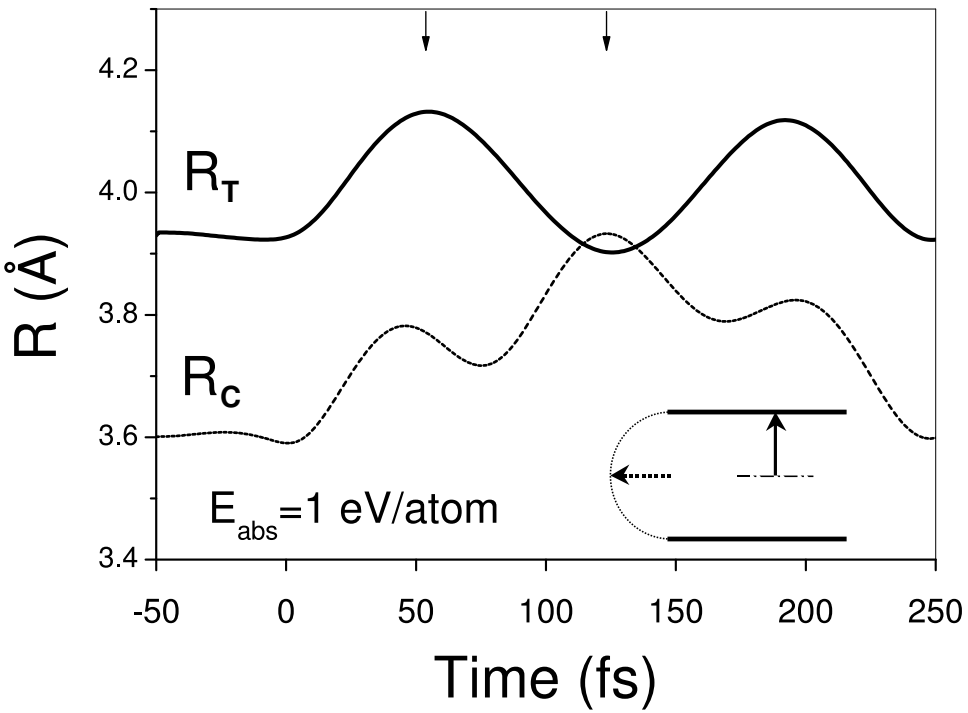

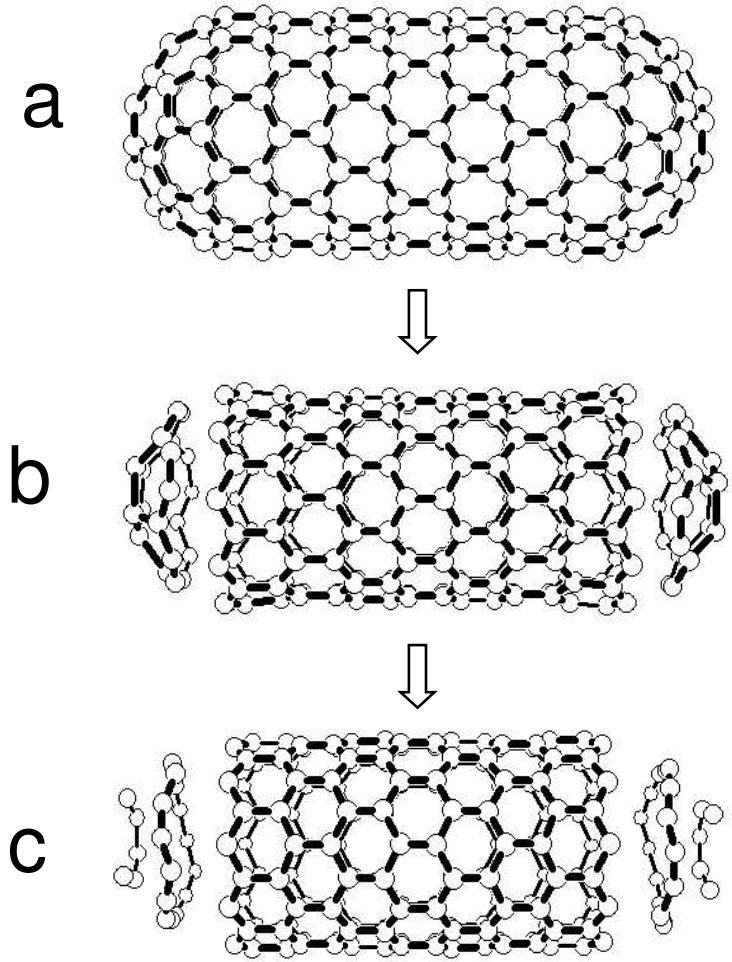

Dumitrica, Garcia, Jeschke, Yakobson, Phys. Rev. Lett. **92**, 117401 (2004).

Laser induced cap opening: Analysis

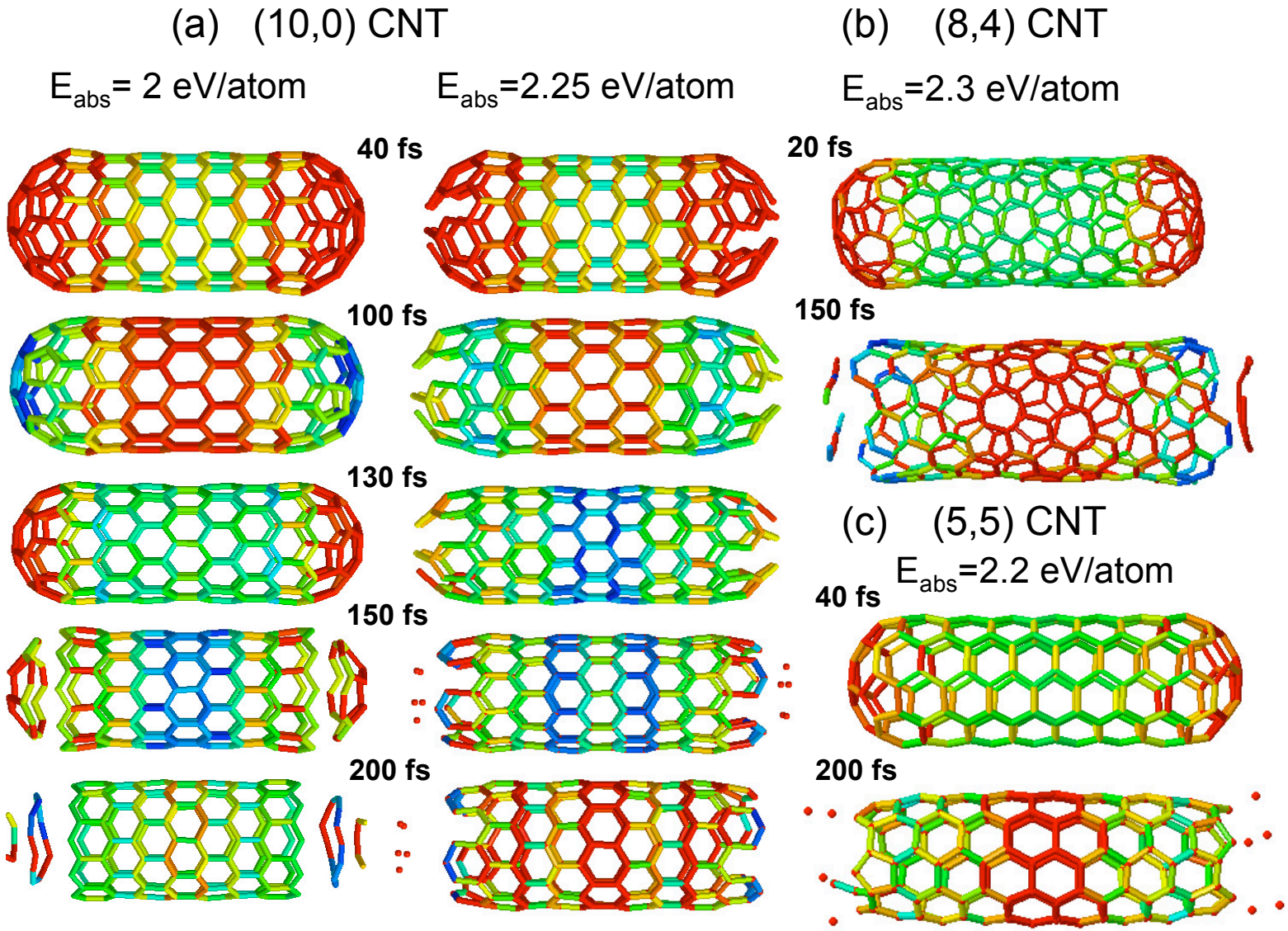

Stone-Wales defect in graphite: Minimum energy path

- Pentgon-heptagon (Stone-Wales) defect in a graphene sheet: one carbon dimer rotated by 90° with respect to regular position.
- Climbing image nudged elastic band (CI-NEB) method based on DFT description yields minimum energy path for defect elimination.

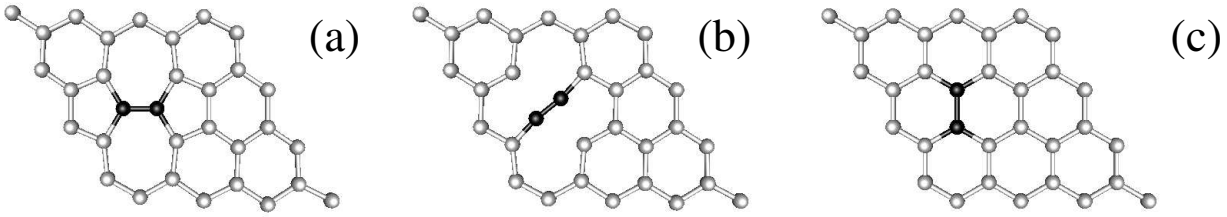

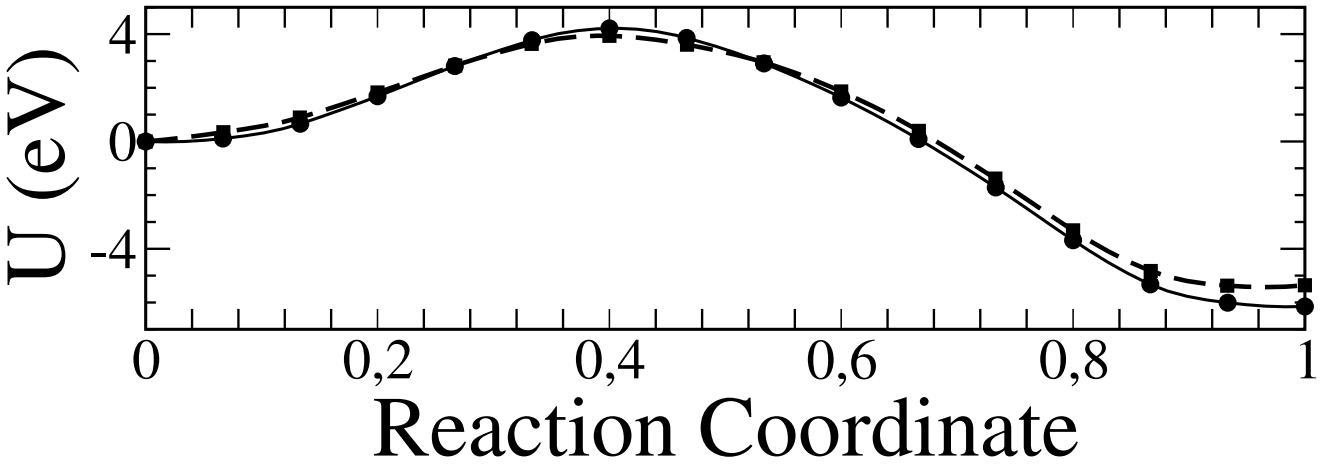

- Barrier of $E_b \approx 4$ eV means high thermal stability of defect.
- Barrier well reproduced with TB (dashed).

Stone-Wales defect in graphite: Laser healing

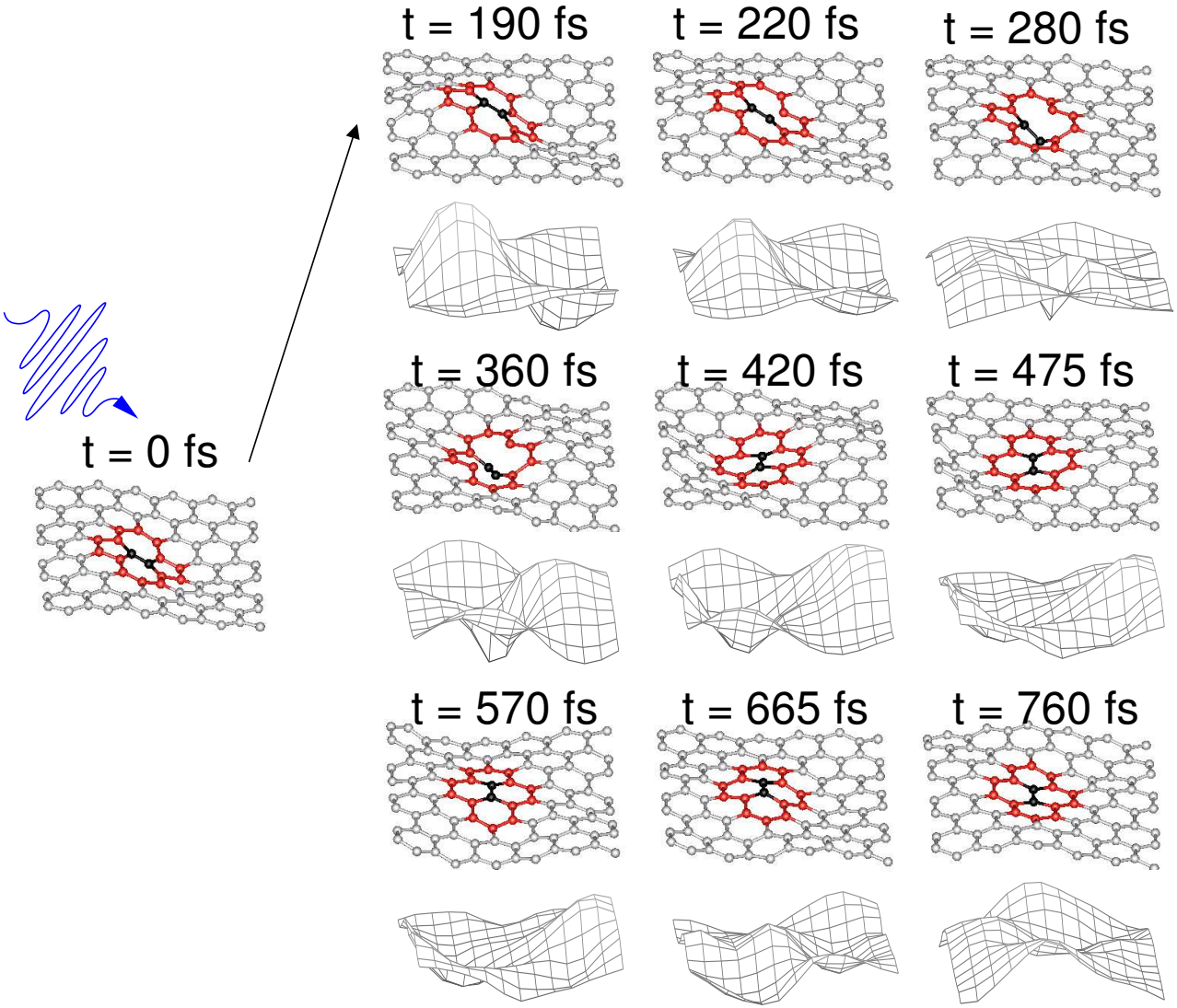

- Laser excitation of 6% of valence electrons can induce inverse Stone-Wales transition, **healing the defect graphene sheet**!
- Laser strongly enhances out-of-plane vibrations of graphene sheet (overall weakening of C-C bonds).

Mechanism of Stone-Wales defect healing

- Plot of total energy $E_{\rm tot} = E_{\rm band}(\{R_i\}) + \Phi(\{R_i\})$ (repulsive potential Φ) for absorbed energies $E_a = 0.77$ eV to $E_a = 1.32$ eV (red, has defect healing around $t = 300$ fs).

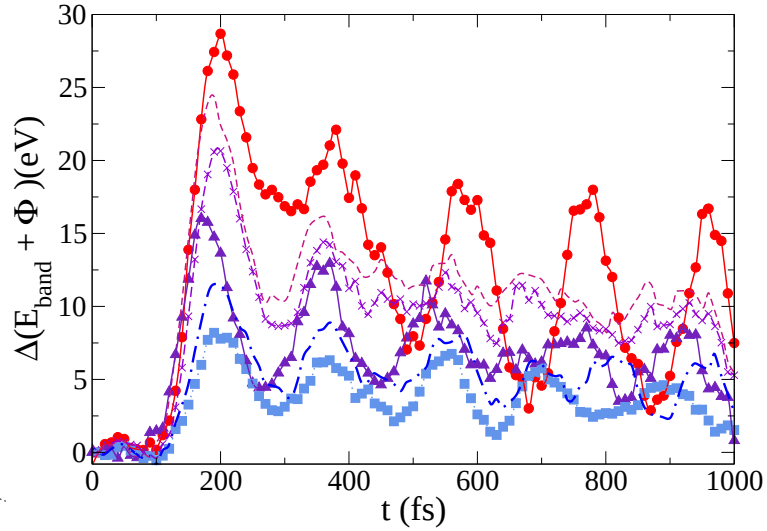

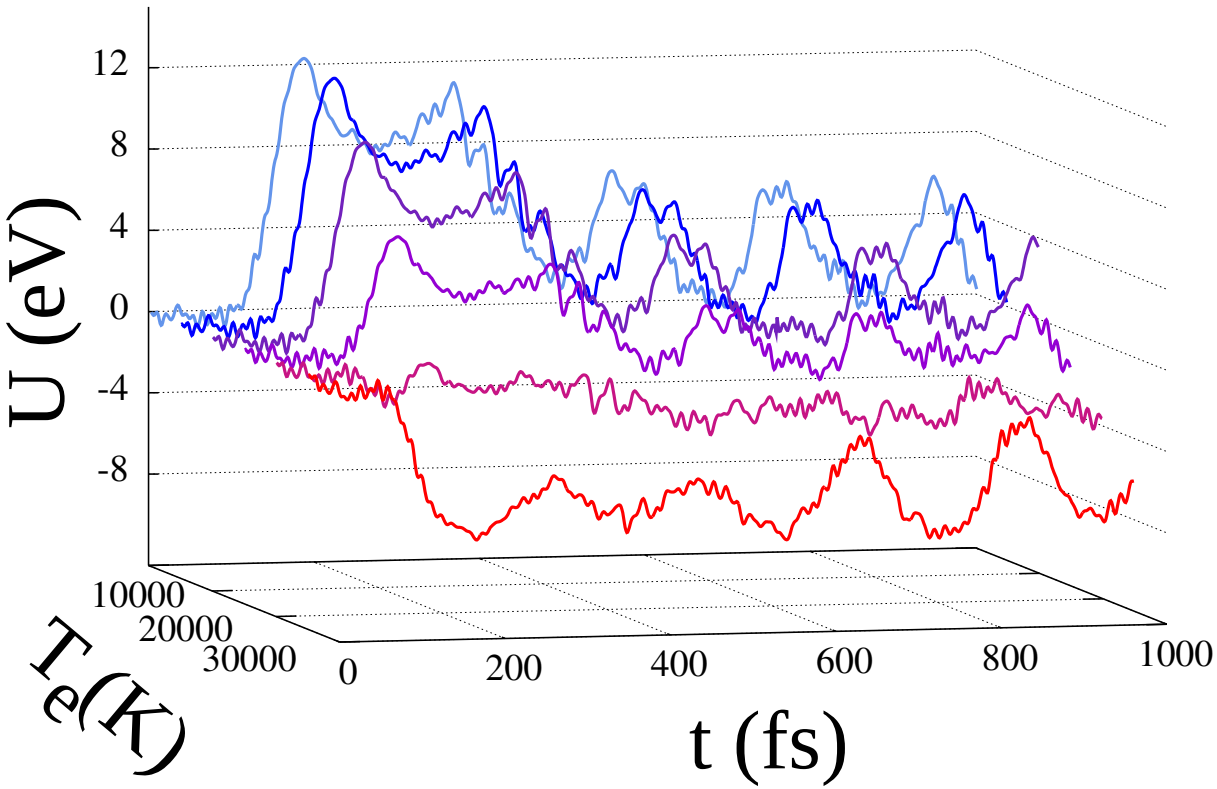

- Free energy $U = E_{\rm tot} - T_e(n_l)S_e(n_l)$ along healing trajectory for different electron temperatures: **Transition is entropy driven!**

Valencia, Romero, Jeschke, Garcia, Phys. Rev. B (2006), in press.

Laser healing of Stone-Wales defect in armchair nanotube

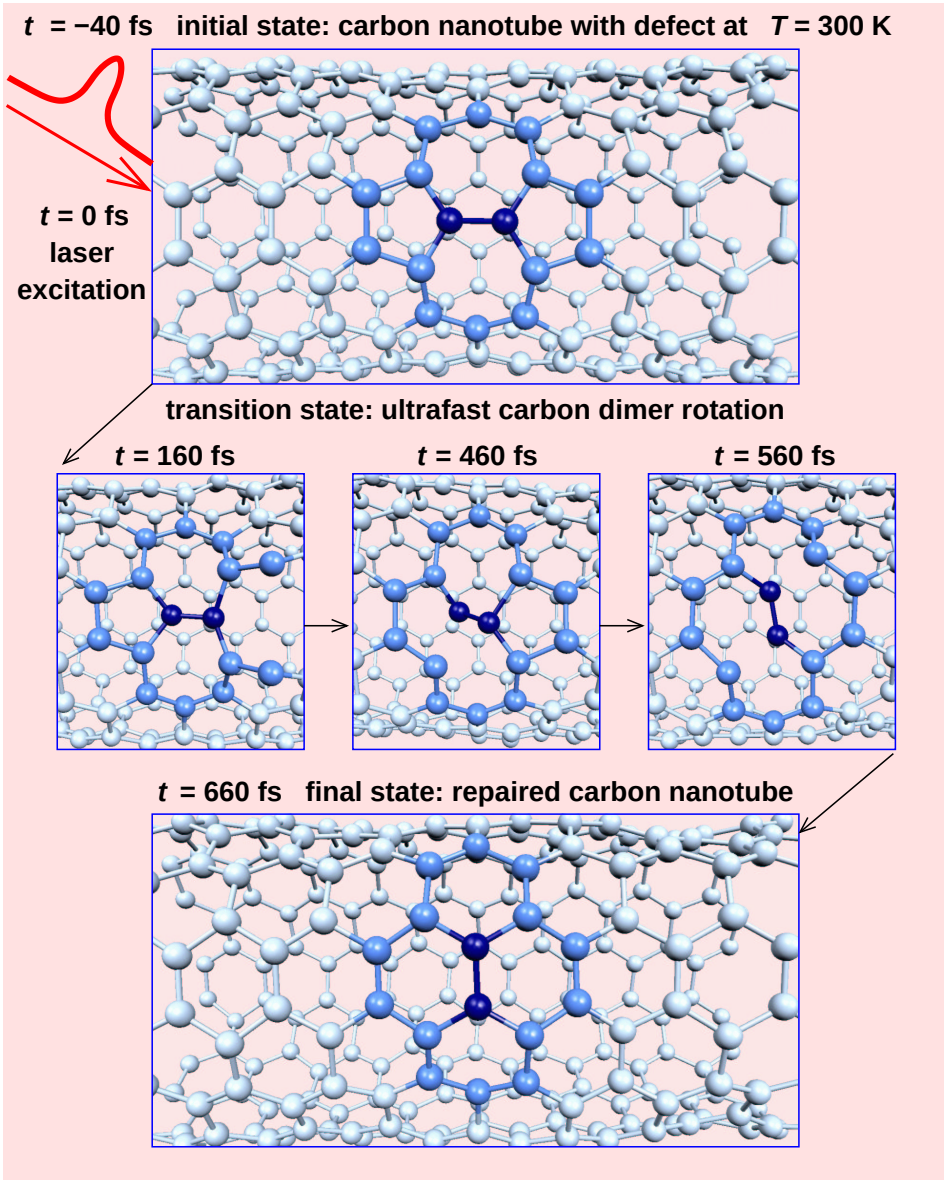

- Mechanism of defect elimination in SWNTs is the similar as in graphene sheet.
- Laser excites radial breathing mode of CNT, facilitating bond breaking in the defect region.
- Important out of plane component of dimer rotation: here, dimer dives into the tube.

Romero, Garcia, Valencia, Terrones, Terrones, Jeschke, Nano Lett. **5**, 1361 (2005).

Laser healing of Stone-Wales defect in zigzag nanotube

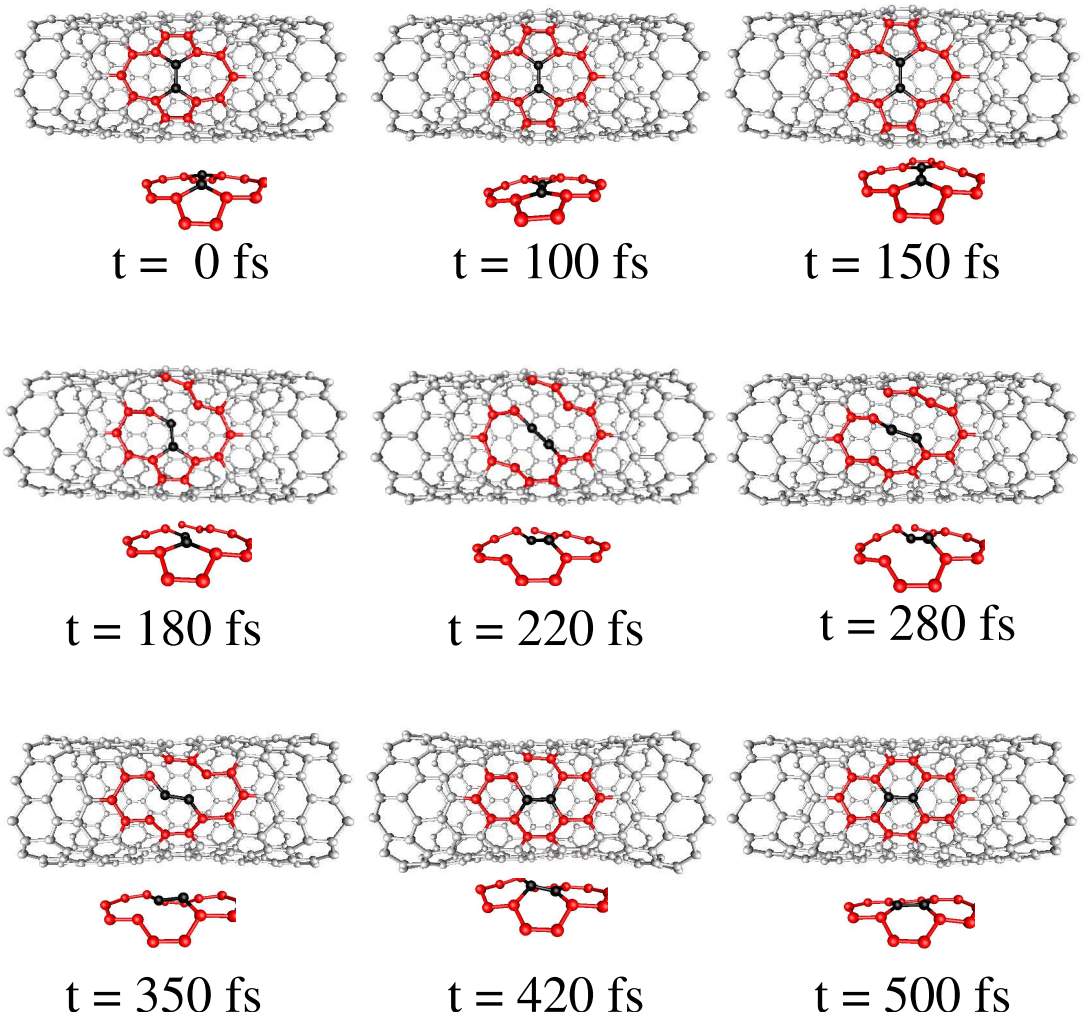

- Defect healing also observed in zigzag nanotubes. (different orientation of irregular dimer with respect to CNT axis). **General effect!**
- Possible explanation for ten times enhanced resonant Raman signal after laser irradiation: Theoretical results supply a microscopic explanation for suspected annealing effect!

Conclusions/Outlook

- SWNT damage thresholds: Nonmonotonous dependence of SWNT damage thresholds on geometry suggests possibility of controlled CNT ensemble manipulation: Laser purification of CNT bundles?
- Nanodiamonds: Laser allows efficient formation of fullerene-like structures.
- Capped nanotubes: Laser excitation of coherent phonons allows precise structural modification. Possibly more generally useful?
- CNTs with defects: Laser pulse induces entropy driven defect elimination. Laser induced nonequilibrium represents fascinating way to manipulate nanostructures.

Work in progress:

- Improved treatment of electronic system (inclusion of chirp, matrix elements).
- Laser welding of CNTs to make junctions.

Publications/Acknowledgments

SWNT damage thresholds:

A. H. Romero, H. O. Jeschke, A. Rubio and M. E. Garcia *Atomistic simulation of the laser induced damage in single wall carbon nanotubes: Diameter and chirality dependence*, Appl. Phys. A **79**, 899 (2004).

H. O. Jeschke, A. H. Romero, A. Rubio and M. E. Garcia, *Microscopic investigation of laser induced structural changes in single wall carbon nanotubes*, to be submitted to Phys. Rev. B (2006).

Nanodiamonds:

A. H. Romero, H. O. Jeschke, and M. E. Garcia, *Laser Manipulation of Nanodiamonds*, Com. Mat. Sci. **35**, 179 (2006).

Capped nanotubes:

T. Dumitrica, M. E. Garcia, H. O. Jeschke and B. I. Yakobson, *Selective cap opening in carbon nanotubes driven by laser-induced coherent phonons*, Phys. Rev. Lett. **92**, 117401 (2004).

T. Dumitrica, M. E. Garcia, H. O. Jeschke and B. I. Yakobson, *Breathing coherent phonons and caps fragmentation in carbon nanotubes following ultrafast laser pulses*, submitted to Phys. Rev. B (2006).

CNTs with defects:

A. H. Romero, M. E. Garcia, F. Valencia, H. Terrones, M.Terrones, and H. O. Jeschke, *Femtosecond Laser Nanosurgery of Defects in Carbon Nanotubes*, Nano Lett. **5**, 1361 (2005).

F. Valencia, A. H. Romero, H. O. Jeschke, M. E. Garcia, *Large amplitude coherent phonons and inverse Stone-Wales transitions in graphitic systems with defects interacting with ultrashort laser pulses*, submitted to Phys. Rev. B (2006).

Collaborators:

Martin Garcia (Uni Kassel), Aldo Romero (CINVESTAV, Mexico), Traian Dumitrica (Univ. Minnesota, USA), Felipe Valencia (Univ. di Padova, Italy).